Sea-to-air CO_2 flux from 1948 to 2003: A model study

P. Wetzel
Max Planck Institute for Meteorology, Hamburg, Germany

A. Winguth
Center for Climatic Research, University of Wisconsin-Madison, Madison, Wisconsin, USA

E. Maier-Reimer
Max Planck Institute for Meteorology, Hamburg, Germany

Received 14 July 2004; revised 10 December 2004; accepted 7 February 2005; published 6 April 2005.

[1] Trends and variability in the ocean-atmosphere CO_2 flux and the uptake of anthropogenic CO_2 are simulated for the period 1948–2003, using a biogeochemical carbon cycle model (HAMOCC5) coupled online to a global ocean general circulation model (MPI-OM). The model is forced by daily National Centers for Environmental Prediction/National Center for Atmospheric Research (NCEP/NCAR) reanalysis data from 1948 to 2003. We find a global interannual variability of ±0.50 PgC yr^{-1} (2σ) which is largely dominated by ocean dynamics in the equatorial Pacific. On decadal scale, two patterns are of global importance. First, the regime shift that occurs in 1975–1977 when the modeled interannual variability of the equatorial Pacific changes from ±0.32 PgC yr^{-1} to ±0.23 PgC yr^{-1} and the mean outgasing of CO_2 decreases from 0.70 PgC yr^{-1} to 0.58 PgC yr^{-1}. Second, the trend that occurs in the Southern Ocean, where we find an increase of the CO_2 fluxes over the full 56-year simulation period. The flux results from stronger upwelling and deeper mixed layers which are caused by increasing wind velocities. We estimate an average CO_2 flux into the ocean of 1.49 PgC yr^{-1} for 1980–1989 and 1.74 PgC yr^{-1} for 1990–1999, with extremes of 1.20 PgC yr^{-1} at the La Niña event in 1996 and 2.10 PgC yr^{-1} during the El Niño events in 1993 and 1998. Because of the rising buffer factor, the uptake of anthropogenic CO_2 is slowing down in regions of shallow mixing toward the end of the simulation. Overall, about 124 Pg of anthropogenic carbon has accumulated in the model ocean until the end of 2003.

Citation: Wetzel, P., A. Winguth, and E. Maier-Reimer (2005), Sea-to-air CO_2 flux from 1948 to 2003: A model study, *Global Biogeochem. Cycles*, *19*, GB2005, doi:10.1029/2004GB002339.

1. Introduction

[2] The CO_2 concentration in the atmosphere has been measured for more then 5 decades [*Keeling and Whorf*, 2002]. The strongest signal in this data set is the increase of CO_2 due to the combustion of fossil fuel, cement production, and land use change. About half of those anthropogenic emissions stay in the atmosphere; the other half is taken up by the ocean and the terrestrial biosphere. Various methods have been employed to constrain the CO_2 fluxes. *Intergovernmental Panel on Climate Change* (*IPCC*) [2001] uses atmospheric O_2/N_2 observations [*Keeling and Shertz*, 1992] to derive the rates of anthropogenic CO_2 uptake. Another common technique is the calculation of the land and ocean CO_2 fluxes from atmospheric CO_2 data with an inverse atmospheric transport model [*Rödenbeck et al.*, 2003; *Gurney et al.*, 2002].

[3] The oceanic uptake of anthropogenic CO_2 can be also estimated from global chlorofluorocarbon (CFC) data sets [*McNeil et al.*, 2003] or observations of the reduced isotopic ratio (^{13}C) of dissolved inorganic carbon (DIC) [*Gruber and Keeling*, 2001]. The Ocean Carbon Cycle Intercomparison Project (OCMIP-2) has evaluated a suite of 19 ocean carbon cycle models with radiocarbon and CFC-11 data [*Matsumoto et al.*, 2004]. Results from those studies are summarized and compared to this study in Tables 1 and 2.

[4] In addition to the anthropogenic increase in CO_2, the atmospheric data shows high natural variability on interannual and decadal timescales. The natural variability is larger than the changes in emissions and is mainly caused by variations in land and ocean carbon cycle. An overview is given in the IPCC report on climate change [*IPCC*, 2001]. The high complexity of the land and ocean carbon cycles, coupled by the atmosphere, makes it very difficult to decon-

0886-6236/05/2004GB002339$12.00

Table 1. Estimated Uptake of Anthropogenic CO_2[a]

Time Span	This Study	CFC Data[b]	OCMIP-2[c]	^{13}C Inventory
1980–1989	−1.67	−1.6 ± 0.4	−1.9 ± 0.2	
1990–1999	−1.93	−2.0 ± 0.4	−2.2 ± 0.2	
1970–1990				−2.1 ± 0.9[d]
1985–1995				−1.5 ± 0.9[e]

[a]In PgC yr^{-1}.
[b]*McNeil et al.* [2003].
[c]*Matsumoto et al.* [2004].
[d]*Heimann and Maier-Reimer* [1996].
[e]*Gruber and Keeling* [2001].

volute the land and the ocean component. Understanding the crucial factors of the flux variability will lead to a better understanding of the mechanisms behind the CO_2 sources and sinks and may be a way to quantify their present and future behavior.

[5] Similar to estimates of the oceanic uptake of CO_2, the estimates of the interannual variability of the sea-to-air CO_2 flux differ considerably. Studies combining CO_2, $\delta^{13}C$, and O_2 data indicate a sea-to-air flux variability of ±1.0–2.5 PgC yr^{-1}, but all with a high uncertainty [*Joos et al.*, 1999; *Rayner et al.*, 1999; *Keeling et al.*, 1995; *Francey et al.*, 1995]. Studies based on variations of the sea surface temperatures and CO_2 partial pressure [*Lee et al.*, 1998; *Feely et al.*, 1999] indicate a much lower variability below, ±0.5 PgC yr^{-1}. A lower estimate is generally supported by ocean model simulations [*Winguth et al.*, 1994; *Le Quéré et al.*, 2000; *Obata and Kitamura*, 2003; *McKinley et al.*, 2004]. The $\delta^{13}C$ signal and terrestrial studies [*Zeng et al.*, 2005] clearly indicate a dominant role of the terrestrial biosphere for the variability. However, *Keeling et al.* [1995] suggest that a considerable sea-air gas exchange, mostly anti-correlated to the terrestrial flux, is needed to explain the atmospheric CO_2 signal. Recent atmospheric inversion estimates [*Rödenbeck et al.*, 2003] show an oceanic interannual variability that is more in line with the ocean model studies.

[6] In this paper we use a biogeochemistry model embedded in a state of the art ocean general circulation and sea ice model. The model is started from a mean state which is fully consistent with the forcing conditions in 1948. From 1948 until 2003, it is driven by a consistent set of atmospheric data with trends and variability on interannual and decadal scales. In addition to the "natural" CO_2 fluxes, we also simulate the effect of rising atmospheric CO_2 concentrations. This enables us to go beyond the work others have done before, and analyze the physical and biological processes that drive the trend and the variability of air-sea CO_2 fluxes and the uptake of anthropogenic CO_2 on interannual and decadal timescales.

[7] This paper is structured in following way. First, we briefly describe the ocean and the biogeochemical model. Section 3 deals with the large-scale mechanisms of natural CO_2 sea-to-air flux variability and uptake of anthropogenic CO_2. In section 4 we focus closer on the processes that determine the carbon exchanges in the equatorial Pacific, the Southern Ocean, and the North Atlantic. Section 5 is a summary and conclusion.

2. Model Description

2.1. Ocean General Circulation Model

[8] The Max-Planck-Institute ocean model (MPI-OM) is a primitive equation model (z-level, free surface), with hydrostatic and Boussinesq assumptions. Transport is computed with the a second-order total variation diminishing (TVD) scheme [*Sweby*, 1984]. The model includes isopycnal diffusion of the thermohaline fields as well as eddy-induced transport by a Gent and McWilliams parameterization [*Gent et al.*, 1995]. Sea ice is modeled with a viscous-plastic rheology following *Hibler* [1979]. The model works on an orthogonal curvilinear C-grid. In this setup, one pole is located over Greenland and the other over Antarctica. The horizontal resolution gradually varies from 20 km in the Arctic to about 350 km in the tropics. It has 40 vertical levels with level thickness increasing with depth. Eight layers are within the upper 90 m, and 20 are within the upper 600 m. The time step is 2.4 hours. For details on MPI-OM and the grid versions, see *Marsland et al.* [2003].

2.2. Carbon Cycle Model

[9] The Hamburg oceanic carbon cycle model (HAMOCC5) is coupled online to the circulation and diffusion of the MPI-OM, running with the same vertical and horizontal resolution and the same time step. Thermohaline fields and biochemical tracers are transported with the same advection scheme. The carbon cycle is based on the HAMOCC3 version of *Maier-Reimer* [1993] and is

Table 2. Sea-to-Air Flux of CO_2 Into the Northern Hemisphere, Tropics, and the Southern Hemisphere in PgC yr^{-1}

	Time Span	South ≤20, PgC yr^{-1}	Tropics, PgC yr^{-1}	North ≥20, PgC yr^{-1}	Total, PgC yr^{-1}
CR experiment	1980–1999	−0.11	1.18	−0.88	+0.18
AR experiment	1980–1989	−0.90	0.65	−1.26	−1.50
	1992–1996	−1.00	0.54	−1.32	−1.78
	1996–1999	−1.03	0.60	−1.29	−1.72
	1995	−1.05	0.64	−1.34	−1.75
Rödenbeck et al. [2003]	1980–1989				−1.2 ± 0.3
	1990–1996	−1.0 ± 0.1	0.9 ± 0.2	−1.6 ± 0.1	−1.7 ± 0.3
	1996–1999	−1.2 ± 0.2	1.1 ± 0.2	−1.7 ± 0.1	−1.7 ± 0.4
Gurney et al. [2002]	1992–1996	−0.9 ± 0.7	0.5 ± 0.6	−1.1 ± 0.4	−1.5 ± 0.4
Takahashi et al. [2002][a]	1995	−1.51	0.90	−1.03	−1.64
IPCC [2001]	1980–1989				−1.9 ± 0.6
	1990–1999				−1.7 ± 0.5

[a]Corrected fluxes using the *Wanninkhof* [1992] gas transfer coefficient (www.ldeo.columbia.edu/CO2/).

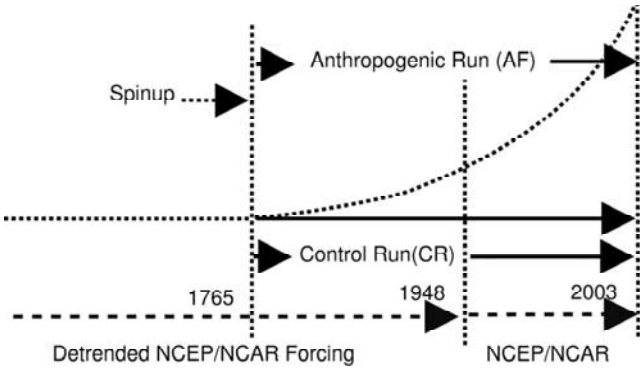

Figure 1. Schematic setup of the control run (CR) and the anthropogenic run (AR).

similar to those of *Winguth et al.* [1994] and *Le Quéré et al.* [2000]. The ecosystem model is based on nutrients, phytoplankton, zooplankton, and detritus (NPZD-type), as described by *Six and Maier-Reimer* [1996]. In addition new elements such as nitrogen, dissolved iron, and dust are accounted for, and new processes like denitrification and N-fixation, formation of calcium carbonate and opaline shells, DMS production, dissolved iron uptake and release by biogenic particles and dust deposition and sinking are implemented. The model contains a sediment module following *Heinze et al.* [2003], including opal, silt, organic carbon, and calcium carbonate. We assume no CO_2 fertilization in the model, so that the biological production is not directly affected by increasing CO_2. The sea-air CO_2 exchange is calculated according to *Wanninkhof* [1992]. Dust input is a climatology of monthly means from a nudged model simulation with ECHAM4 by *Timmreck and Schulz* [2004]. We assume a 1% solubility for atmospheric iron. Phytoplankton assimilates iron with a fixed ratio to phosphate. Iron is regenerated when particulate and dissolved organic carbon (POC and DOC) are remineralized. Iron scavenging is parameterized in analogy to *Johnson et al.* [1997]. This approach assumes that dissolved iron beyond the limit of 0.6 nmol L^{-1} is complexed by strong iron binding ligands and is lost to the biogeochemical cycle. *Aumont et al.* [2003] describe a HAMOCC5 version that is also derived from HAMOCC3. In contrast to the model used in this study, their ecosystem is different, and the ocean transport is based on an offline version of the Hamburg Large Scale Geostrophic (LSG) model [*Maier-Reimer*, 1993]. A detailed technical description of HAMOCC5 will be available as a MPI-report in spring 2005 [*Maier-Reimer and Kriest*, 2005].

2.3. Model Initialization and Forcing

[10] The model is forced using daily heat, freshwater, and momentum fluxes computed from the NCEP/NCAR reanalysis [*Kalnay et al.*, 1996]. In ice-free regions, surface salinity (upper 12 m) is relaxed toward the Levitus climatology [*Conkright et al.*, 1998] with a time constant of 180 days. The ocean model is initialized from the Levitus climatological temperature and salinity data [*Conkright et al.*, 1998]. The biogeochemical model is started with an uniform tracer distribution.

[11] The NCEP/NCAR reanalysis includes the global warming signal. To get a best estimate of the initial conditions, consistent with the beginning of the NCEP/NCAR reanalysis period, we have computed a detrended set of the NCEP/NCAR fields from 1948 to 2001 with respect to the reanalysis of 1948. The model was integrated for 1700 years, periodically repeating the forcing with the detrended fields, while the inventory of alkalinity was adjusted to match a preindustrial CO_2 level of 278 ppm. Fluxes and tracer distribution stabilized after about 1000 model years. The patterns of the biochemical tracers are generally consistent with data compilations from observations [*Conkright et al.*, 1998; *Key et al.*, 2004]. Tracers are not restored to data, to be fully consistent with the biological, chemical, and physical dynamics of the model.

[12] From this cyclo-stationary preindustrial state we have started two experiments (Figure 1). A run with rising atmospheric CO_2 levels for the years 1765 to 2003 and an otherwise identical control run with atmospheric CO_2 kept at a preindustrial level of 278 ppm. For the years 1765 to 1947 both experiments are forced with the detrended fields and, from the year 1948 on, with the original NCEP/NCAR fields with included trend. Hereinafter we will refer to the two experiments as the AR (anthropogenic run) and the CR (control run). To extract the oceanic uptake variability from fluctuations caused by varying atmospheric CO_2 concentrations, a smoothed, strictly monotonic increasing atmospheric CO_2 concentration is used. It is taken from a spline fit to ice core and Mauna Loa CO_2 data [*Enting et al.*, 1994] (www.ipsl.jussieu.fr/OCMIP/). In this paper, we only discuss the time span from 1948 to 2003 with the original NCEP/NCAR forcing with all long-term trends included.

[13] Sensitivity tests with different initial conditions at different years have shown that upper layer ocean properties are reasonably adjusted after about 5 years. The direction of the CO_2 flux adjusts almost directly, and the amplitude converges after 5 to 10 years. The timescale corresponds to the timescale of changes in the main thermocline in the equatorial Pacific. In this paper we focus on the interpretation of the years 1948 to 2003, which are computed with the non-detrended NCEP/NCAR reanalysis forcing fields. The first model years should not be interpreted as they are influenced by the last years of the previous (detrended) forcing period. In addition, the first years of the NCEP/NCAR reanalysis suffer from the sparseness of the database.

3. Global Patterns

3.1. CO_2 Fluxes and Variability

[14] The global average CO_2 fluxes for the year 1995 from the anthropogenic run (AR) experiment are shown in Figure 2a. Positive CO_2 fluxes go from the ocean to the atmosphere. Fluxes are dominated by the Ekman-induced upwelling with high outgasing of CO_2 in the equatorial Pacific, Atlantic, and Arabian Sea. The weak CO_2 flux into the ocean in the midlatitudes is mostly due to the cooling of warmer waters flowing to higher latitudes. The high influx in the Southern Ocean and in the northern high-latitude

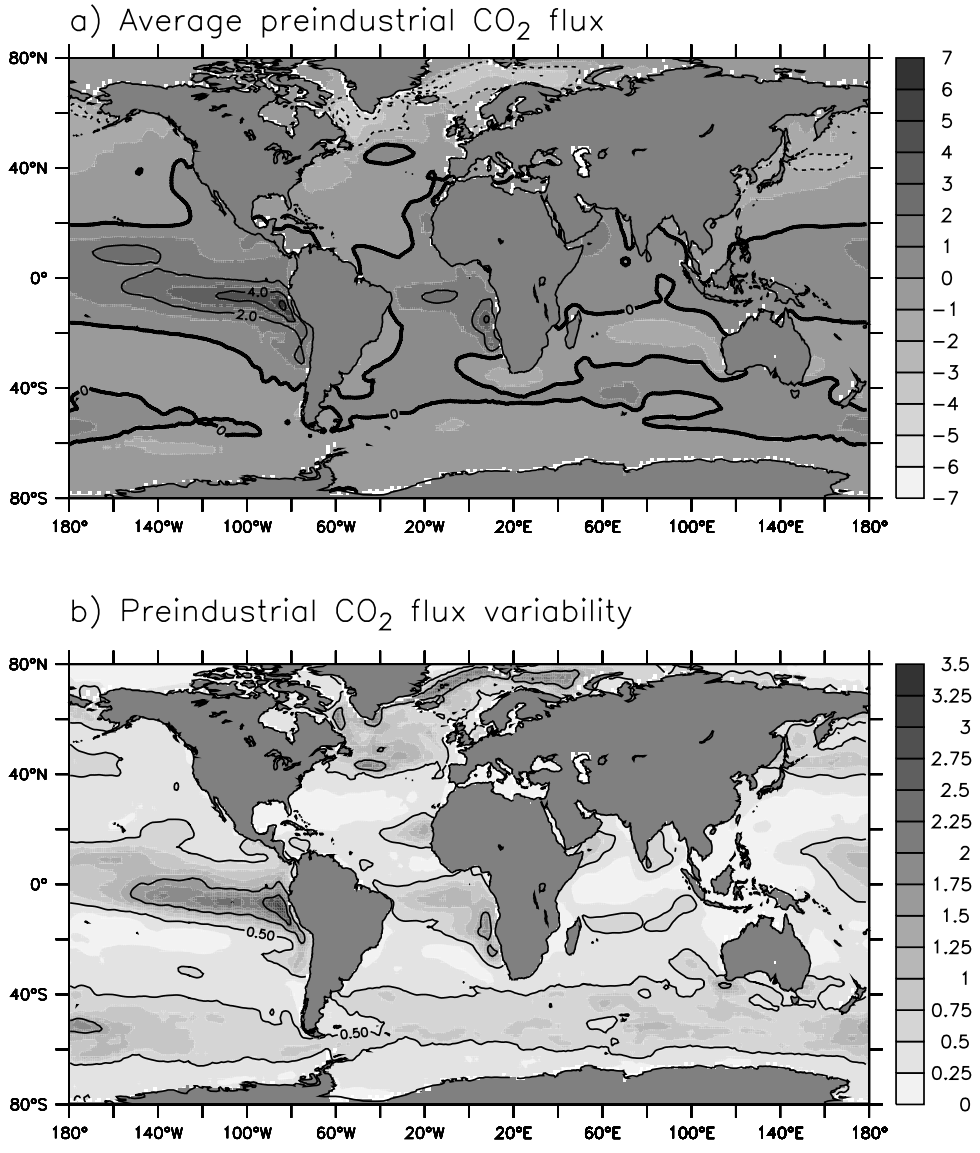

Figure 2. (a) Average CO_2 flux and (b) CO_2 2σ-variability of the control run in PgC yr^{-1}, simulated with MPIOM-HAMOCC5. See color version of this figure at back of this issue.

areas can primarily be attributed to photosynthetic utilization of CO_2 in their respective summers. Uptake of CO_2 is also associated with deep water formation in the Labrador, Greenland, Iceland, and Norwegian seas.

[15] The CO_2 fluxes and the CO_2 partial pressure difference between the ocean and the atmosphere (ΔpCO_2) are tightly connected. In Figure 3, the mean spatial pattern of ΔpCO_2 for the reference year 1995 of the "climatological" data compilation from *Takahashi et al.* [2002] is compared with corresponding values of the year 1995 from the AR experiment. For better comparison the model results are interpolated to the 4° × 5° grid of *Takahashi et al.* [2002]. The modeled pattern agrees reasonably well with the observations, but there are local differences. For example, small areas in the Greenland, Iceland, Norway, and Labrador seas are not well resolved in the course grid of *Takahashi et al.* [2002]. The model shows very low ΔpCO_2 in the areas during the northern summer and a considerable uptake of natural and anthropogenic CO_2. Model and data are generally in good agreement in low latitudes. An exception is the Arabian Sea, where the model underestimates the monsoon induced upwelling. In the Southern Hemisphere this study predicts, in comparison with *Takahashi et al.* [2002], lower ΔpCO_2 south of 50°S and higher ΔpCO_2 between 14°S and 50°S. The seasonal cycle of the model is generally larger than that of *Takahashi et al.* [2002]. The CO_2 fluxes from *Takahashi et al.* [2002] (discussed in sections 3.3 and 4.2) have been derived by multiplying the ΔpCO_2 map with the *Wanninkhof* [1992] gas transfer coefficient (based on the square of the wind speed), using the 10-m wind speed from the NCEP/NCAR reanalysis. In this case, ΔpCO_2 is fixed and the flux is a linear function of the gas exchange coefficient (k).

$$Flux = \Delta pCO_2 \times k. \quad (1)$$

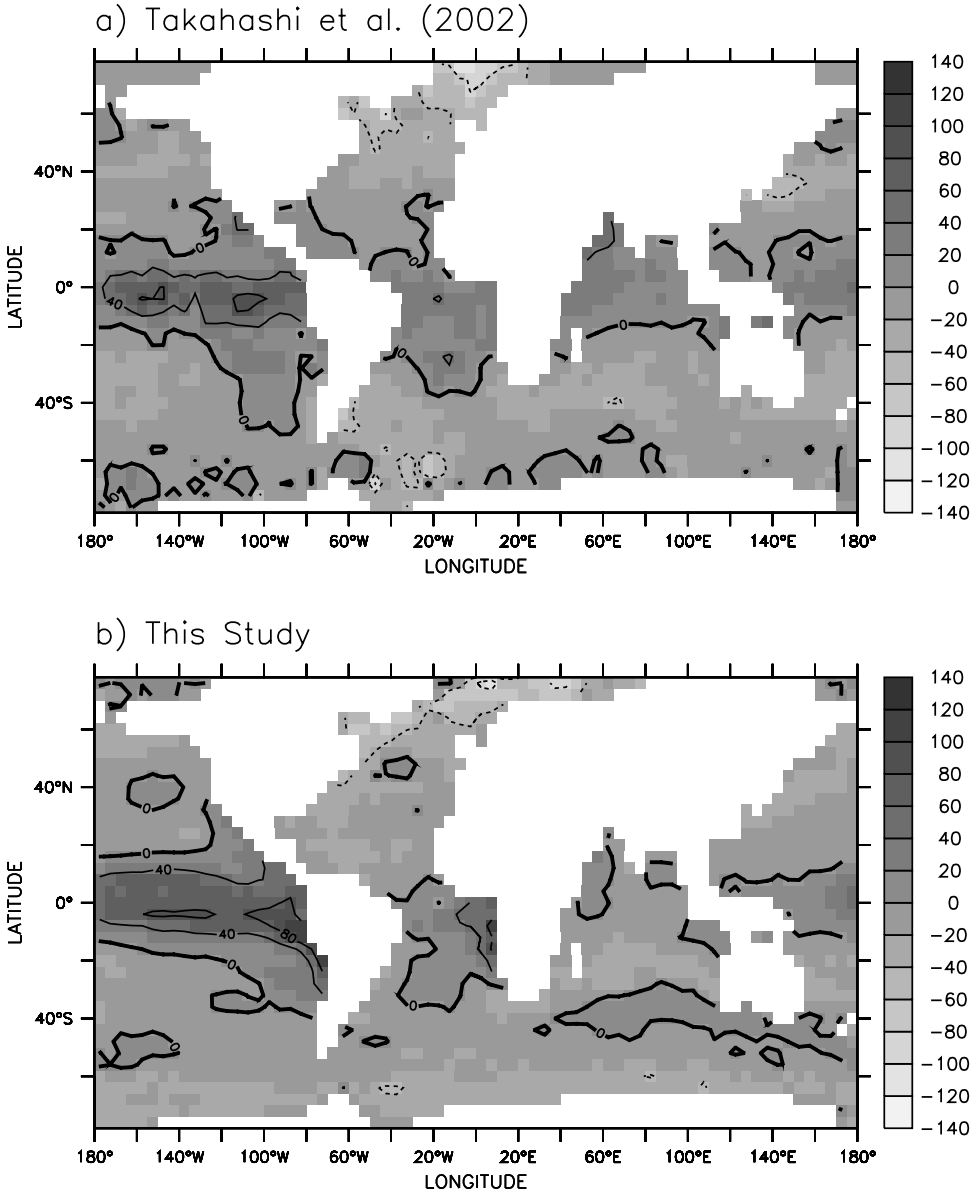

Figure 3. (a) Mean ΔpCO_2 values from *Takahashi et al.* [2002], computed for the reference year 1995 in ppm. (b) Mean ΔpCO_2 of the year 1995 of the anthropogenic run in ppm; interpolated to the $4^\circ \times 5^\circ$ grid of *Takahashi et al.* [2002]. See color version of this figure at back of this issue.

In a carbon cycle model such as HAMOCC5, ΔpCO_2 is a function of the CO_2 flux.

$$\Delta pCO_2 = \frac{Flux}{k}. \tag{2}$$

The flux is generated by inner oceanic processes, i.e., the upwelling of DIC-enriched water. The gas exchange coefficient k only determines the horizontal pattern of ΔpCO_2. The total CO_2 flux is relatively insensitive to the gas exchange parameterization.

[16] Fluxes from the control run (CR) experiment are shown in Figure 4. The global annual CO_2 flux variability for 1948–2003 is ±0.50 PgC yr^{-1} (2σ). The trend originates in the Southern Hemisphere, and is equivalent to an overall atmospheric increase of 4.7 ppm over the 56 years. It is not related to an internal model drift, but it reflects a strengthening in the forcing wind fields.

[17] The global view of the interannual flux variance (Figure 2b) shows three regions of high variability, which will be discussed in detail in section 4. First, the equatorial Pacific which dominates the interannual CO_2 flux variability in our simulation with over 70%. Second, the Southern Ocean which accounts for over 20% of the interannual CO_2 flux variability and, in the AR experiment, for one third of the global uptake of anthropogenic CO_2. It shows the highest trend of all regions throughout the NCEP/NCAR reanalysis period. Third, the deep water formation regions

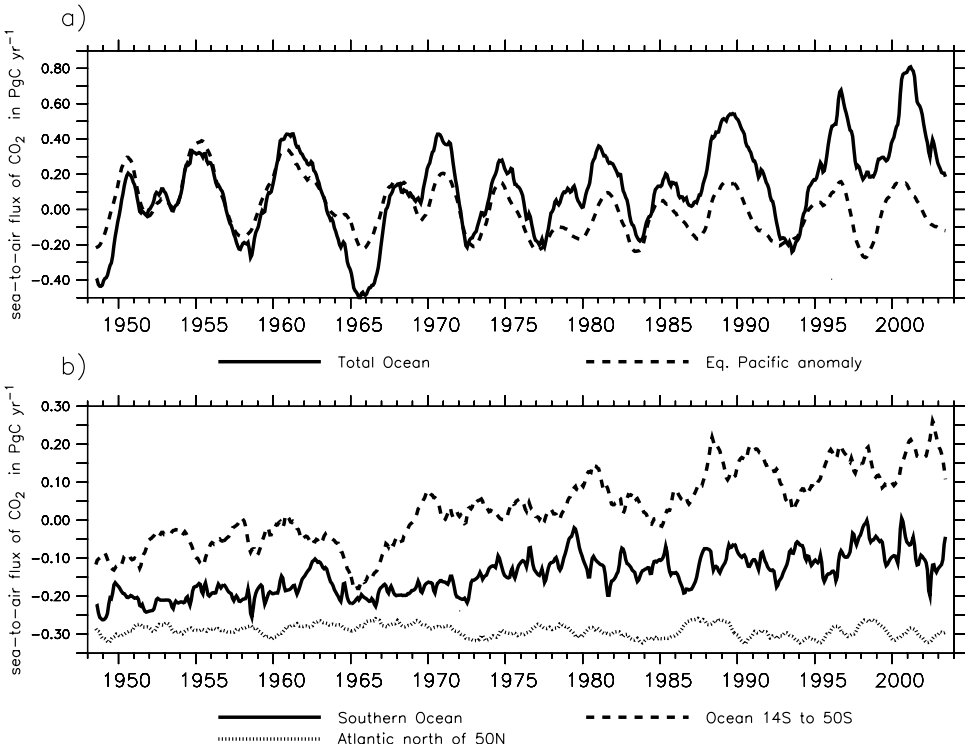

Figure 4. Simulated sea-to-air fluxes of CO_2 in PgC yr^{-1} of the control run (CR), smoothed with a 12-month running mean. (a) CO_2 flux anomaly in the equatorial Pacific and the CO_2 fluxes of the total ocean. (b) CO_2 fluxes for the area from 14°S to 50°S, the Southern Ocean south of 50°S, and the Atlantic north of 50°N.

in the North Atlantic, Greenland, Iceland, and Norwegian seas which are of high importance for the global carbon cycle and characterized by a pronounced seasonal cycle. In addition, regionally, these areas show high interannual variability.

3.2. Anthropogenic CO_2 Uptake

[18] We define the uptake of anthropogenic CO_2 as the difference between the CO_2 fluxes of the AR and the CR experiment. Because of the high variability and the trends in various ocean regions, there is a considerable difference between the CO_2 flux of the AR experiment and the calculated uptake of anthropogenic CO_2. In upwelling regions, uptake of anthropogenic CO_2 means less outgasing compared to the CR. The uptake of anthropogenic CO_2 is high where older waters are mixed to the surface, such as in the northern and southern high latitudes and in the equatorial upwelling regions (Figure 5a). Much of the anthropogenic carbon taken up in the high latitudes and in the upwelling regions is transported to the subtropics and stored there, mostly in the upper few hundred meters of the water column. In the subtropics, with small anthropogenic uptake and low biological productivity, the oceanic CO_2 partial pressure follows the partial pressure of the atmosphere almost directly. The deep water formation areas in the North Atlantic are characterized by a high uptake combined with large storage of anthropogenic CO_2.

[19] Higher CO_2 concentrations are raising the buffer factor and slowing down further uptake (Figure 6). An exception is the Southern Ocean where the constantly increasing wind stress leads to higher mixing. First of all, the slowdown is noticeable in regions with a shallow mixed layer depth. The El Niño events in 1993 and 1998 are clearly recognizable by a decrease in uptake (Figure 6, at about 356 ppm and 364 ppm).

[20] We estimate an average uptake of anthropogenic CO_2 of 1.67 PgC yr^{-1} for 1980–1989 and 1.94 PgC yr^{-1} for 1990–1999. The interannual variability of the uptake of anthropogenic CO_2 is far less then the natural variability of the CO_2 fluxes (Figure 7). The phases of higher uptake mostly reflect deep mixing events in the Southern Ocean, while the decrease in the 1990s is primarily caused by large-scale effects in association with the El Niño events in 1993 and 1998. The model results are consistent with uptake estimates of anthropogenic CO_2 from CFC data [*McNeil et al.*, 2003] and within range of the coarser estimates from the oceanic ^{13}C inventory [*Heimann and Maier-Reimer*, 1996; *Gruber and Keeling*, 2001] (Table 1).

3.3. Anthropogenic CO_2 Fluxes

[21] The effective flux of CO_2 represents the sum of the natural CO_2 fluxes and the uptake of anthropogenic CO_2. Because of the trend of the fluxes of the CR experiment, the total flux of CO_2 into the ocean between 1980 and 2000 is about 0.18 PgC yr^{-1} smaller than the computed uptake of anthropogenic CO_2. The average flux of −1.49 PgC yr^{-1} for 1980–1989 and −1.74 PgC yr^{-1} for 1990–1999 agrees reasonably well with the estimates from atmospheric

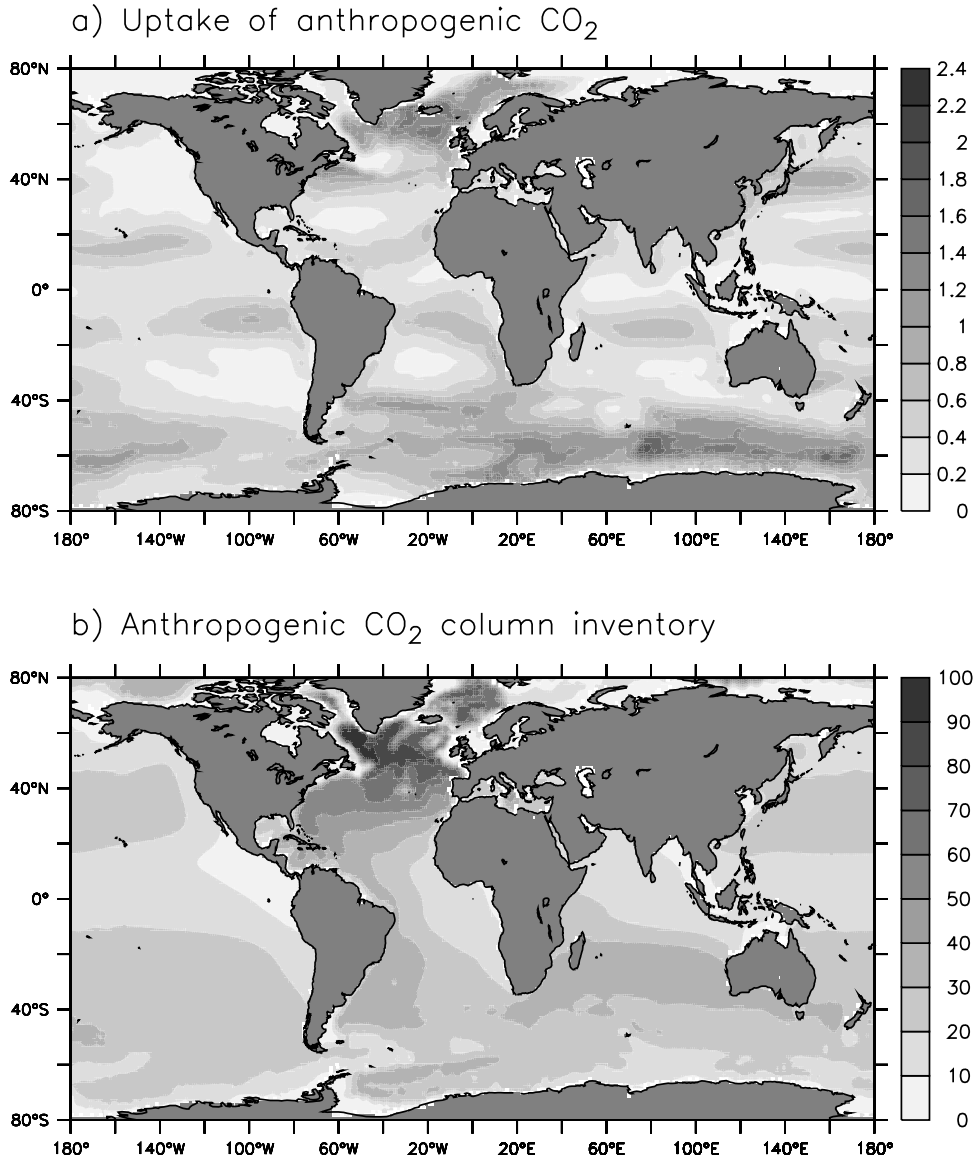

Figure 5. (a) Mean anthropogenic CO_2 uptake for 1990–1999 in mol C m^{-2} yr^{-1}. (b) Mean column inventory of anthropogenic CO_2 of the year 1995 in mol C m^{-2}. See color version of this figure at back of this issue.

inversions [*Rödenbeck et al.*, 2003; *Gurney et al.*, 2002] (Table 2).

[22] In contrast to our results, estimates from O_2/N_2 ratio measurements indicate a decreased CO_2 flux into the ocean from 1980–1989 to 1990–1999 (IPCC report [*IPCC*, 2001]). Their estimates assume a zero net sea-to-air flux of O_2. This assumption may not hold for the period 1980–1999. HAMOCC5 includes O_2 and N_2 as integrated parameters of the biogeochemical cycle. From our simulated O_2 and N_2 fluxes we calculate a interannual variability of the O_2/N_2 correction term of ±0.20 PgC yr^{-1} (2σ). For 1980–1989 and 1990–1999 we find an average net uptake of O_2 which would require a minor reduction of the oceanic flux estimates of *IPCC* [2001] (−0.07 PgC yr^{-1} for 1980–1989 and −0.05 for 1990–1999). *Bopp et al.* [2002] estimate a correction for 1990–1996 of −0.5 PgC yr^{-1} using the observed heat fluxes and a modeled O_2 flux to heat flux relationship. Applying this relationship yields a higher CO_2 flux of −2.3 PgC yr^{-1} for 1990–1999.

3.4. Anthropogenic CO_2 Inventory

[23] Analogous to the uptake of anthropogenic CO_2 in section 3.2, the inventory of anthropogenic carbon is computed as the difference between the dissolved inorganic carbon (DIC) inventory of the AR and the CR experiment. Storage of anthropogenic CO_2 in surface waters is high in areas with a high buffer capacity (Figure 5). High buffer capacity is a consequence of a low buffer factor (or Revelle factor). The buffer factor depends on temperature, alkalinity, and DIC and is generally higher in the cold water of the

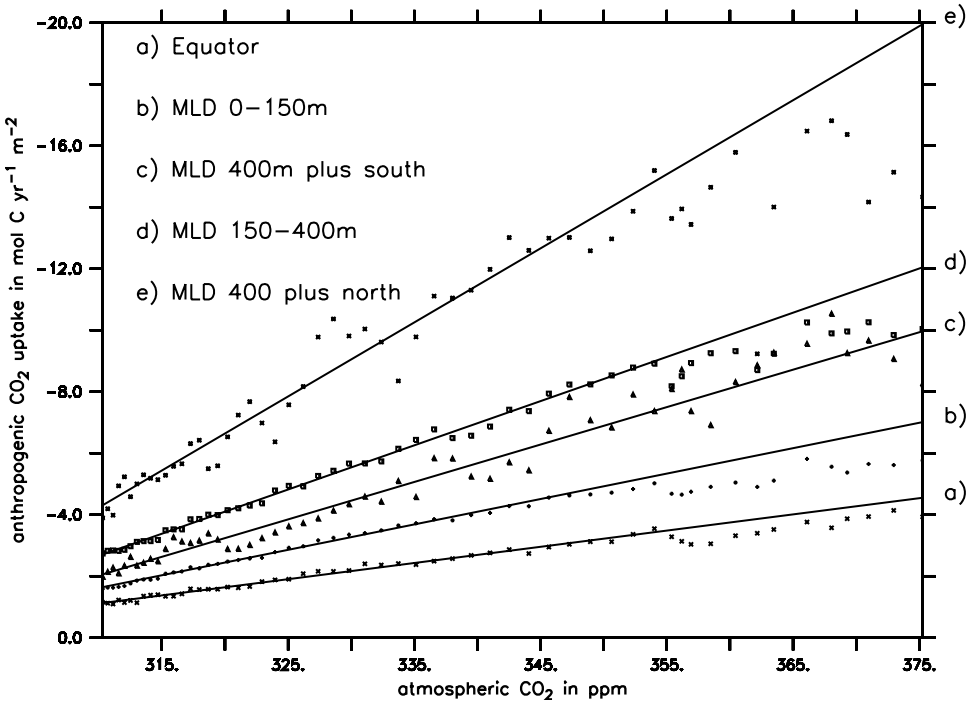

Figure 6. Yearly averages of anthropogenic CO_2 uptake versus atmospheric CO_2 concentrations. The uptake rates are computed for the equatorial regions, regions with an average mixed layer depth of up to 150 m, 150 m to 400 m, and over 400 m in the Northern and Southern Hemisphere. The linear regression lines are computed for 310 ppm to 345 ppm and extended over the full range. See color version of this figure at back of this issue.

high latitudes. Anthropogenic carbon which invades the ocean in the high southern latitudes and the upwelling regions along the equator is mostly transported into the subtropical convergence where it is subducted and accumulates mostly in the upper 1000 m of the water column. Deep entrainment of anthropogenic CO_2 mainly occurs in the deep water formation areas of the North Atlantic. The model also shows some deeper entrainment near the Weddell Sea in the Southern Ocean. In the equatorial regions and elsewhere in the high latitudes, the concentrations of anthropogenic CO_2 are low.

[24] In the model, 124 Pg of anthropogenic carbon accumulated in the ocean until the end of 2003. About 20 PgC have invaded the ocean within the last 10 years. The simulated anthropogenic DIC concentrations and the global spatial distribution for the year 1994 are in good agreement with the estimates by the ΔC technique (Table 3). The "ΔC" technique [*Gruber et al.*, 1996] is a method to separate the small anthropogenic CO_2 signal from the large natural background of DIC. The method uses various measurements of gases and nutrients and involves a number of assumptions about the composition of organic matter. *Lee et al.* [2003] and *Sabine et al.* [2002, 1999] use this technique to estimate an inventory of anthropogenic CO_2 for the Atlantic, the Pacific, and the Indian Ocean. *Sabine et al.* [2004] synthesize the individual ocean estimates to provide a global estimate of the oceanic sink. In the Pacific and the Indian Ocean the simulated inventory almost matches the calculations of *Sabine et al.* [2002, 1999]; however, our estimate for the Atlantic is about 25% lower than the calculation by *Lee et al.* [2003]. The difference may be related to the different approaches of *Sabine et al.* [2002, 1999] and *Lee et al.* [2003] to estimate the air-sea CO_2 disequilibrium term for shallow surfaces. Because of limited data coverage, the mapped regions in the *Sabine et al.* [2004] paper exclude the marginal basins and the Arctic Ocean north of 65°N. Our results in the mapped regions match well with the estimate from *Sabine et al.* [2004]. However, they estimate an additional 12 PgC in the excluded regions, whereas we only find 4.2 PgC.

4. Regional Variability

4.1. Equatorial Pacific

[25] The global interannual CO_2 flux variability is governed by the equatorial Pacific (Figure 4). This result is in agreement with other ocean carbon cycle model studies [*Winguth et al.*, 1994; *Le Quéré et al.*, 2000; *Obata and Kitamura*, 2003; *McKinley et al.*, 2004]. In the control run (CR) experiment, the equatorial Pacific from 10°N to 10°S accounts for ± 0.33 PgC yr^{-1} (2σ), which is about 65% of the global interannual CO_2 flux variability. The equatorial Pacific has a significant share of the interannual variability, because the changes in the ocean dynamics are acting in phase over a large region. During the unusual El Niño events of 1965/1966 and 1991–1994 the correlation between the CO_2 flux and ocean dynamics is pronounced, resulting in the two largest sea-to-air flux minima in the 56-year period of the experiment. The correlation between the fluxes and the Southern Oscillation Index (Figure 8) is

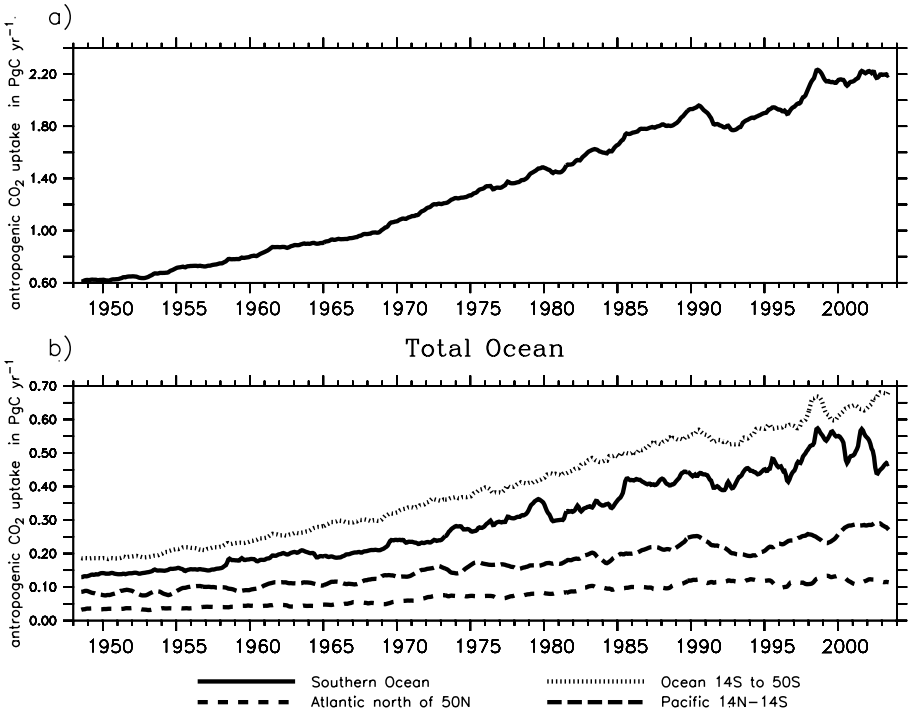

Figure 7. (a) Total anthropogenic CO_2 uptake in PgC yr^{-1}. (b) Uptake for various ocean regions in PgC yr^{-1}. Results from the anthropogenic run smoothed with a 12-month running mean.

0.69 on average and up to 0.95 in the central equatorial Pacific. In general, the other ocean regions are characterized by counteracting dynamical, chemical, and biological processes, which result in an overall weak signal in the air-to-sea CO_2 flux anomalies.

[26] The variability of dissolved inorganic carbon (DIC), temperature (T), total alkalinity (ALK), salinity (S), and the biological productivity is controlled by the trade-wind driven, Ekman-induced upwelling. The upwelled waters from below are cold, rich in nutrients and DIC, and of higher salinity and alkalinity than the surface waters. The magnitude of the CO_2 flux depends on the gas exchange and ΔpCO_2. The ΔpCO_2 is dominantly affected by DIC, T, ALK, and S. The relative importance of the different components can be quantified by a component analysis [*Takahashi et al.*, 1993]. The total derivative of pCO_2 with respect to time can be written as

$$\frac{dpCO_2}{dt} = \frac{\partial pCO_2}{\partial \mathrm{DIC}}\frac{d\mathrm{DIC}}{dt} + \frac{\partial pCO_2}{\partial T}\frac{dT}{dt} + \frac{\partial pCO_2}{\partial \mathrm{ALK}}\frac{d\mathrm{ALK}}{dt} + \frac{\partial pCO_2}{\partial S}\frac{dS}{dt}. \quad (3)$$

[27] Analogous to *Le Quéré et al.* [2000], Figure 9a shows all terms of equation (3) except salinity, which only has a minor direct influence on pCO_2. The effects of temperature and alkalinity are of similar magnitude and directly anti-correlated to DIC. Together they damp the pCO_2 variability by about 50%. The changes in alkalinity are for the most part influenced by fresh water fluxes. Normalizing the changes in DIC and alkalinity to salinity almost cancels the alkalinity term of equation (3); the DIC term of equation (3) changes likewise, so the sum of both remains. The variation of the DIC concentration can be written as a linear combination of sources and sinks,

$$\frac{d\mathrm{DIC}}{dt} = J_{\mathrm{adv}} + J_{\mathrm{dif}} + J_{\mathrm{wf}} + J_{\mathrm{co2}} + J_{\mathrm{bio}}. \quad (4)$$

[28] J_{adv} and J_{dif} represent the transport by ocean advection and the mixing by diffusion, and J_{wf} is the dilution or concentration from fresh water fluxes. The air-sea exchange of CO_2 and uptake by biological production are represented by J_{co2} and J_{bio}. A positive sea-to-air flux as well as biological carbon export leads to a lower DIC concentration, and hence corresponds to negative J_{co2} and J_{bio}, respectively. The influence of J_{co2} and J_{bio} on the total variation is about 25% of (J_{adv}), each. J_{wf} and J_{dif} show no clear correlation and are of lesser importance. The relatively low biological productivity in the equatorial Pacific can result from iron limitation [*Chavez et al.*, 1999; *Coale et al.*, 1996]. In the model, the fairly small influence of the biological production on the variability of DIC is related to the limitation by iron. *Obata and Kitamura* [2003] suggested that incorporating such a limitation would increase the CO_2 flux variability, but results from a sensitivity study with this model show a 35% decrease of the CO_2 flux variability in the equatorial Pacific, due to the limitation by iron. First, an almost complete utilization of all upwelled nutrients within the equatorial region ultimately leads to a higher export and more remineralization of organic material and hence to a higher nutrient and DIC

Table 3. Anthropogenic Carbon Inventory in PgC

	South of Equator	North of Equator	South of 35°S	North of 35°S	Total
		Atlantic Ocean (1994)			
Lee et al. [2003]	18.5 ± 3.9	28.4 ± 4.7			46.9 ± 8.6
This study (1994)	13.3	23.1			36.4
		Pacific Ocean (1994)			
Sabine et al. [2002]	28.0	16.5			44.5 ± 5.0
This study (1994)	27.0	17.5			44.5
		Indian Ocean (1995)			
Sabine et al. [1999]			13.6 ± 2.0	6.7 ± 1.0	20.3 ± 3.0
This study (1995)			13.6	7.4	21.0
		Total Ocean (1994)			
Sabine et al. [2004]					
Mapped area (1994) [a]					106 ± 17
Total estimate (1994)					118 ± 19
This study					
Mapped area (1994)[b]					100.1
Total ocean (1994)	57.6	46.7			104.3
Total ocean (1995)	58.6	47.5			106.2

[a]Excluding marginal basins and Arctic Ocean north of 65°N.
[b]Model result for the mapped area of *Sabine et al.* [2004].

concentration underneath the equator. Strong upwelling events, associated with, for example, La Niña events, bring the accumulated DIC to the surface, causing a strong outgasing of CO_2 from the ocean to the atmosphere. Second, the complete utilization of nutrients is resulting in very low oceanic pCO_2 during times of weak upwelling, associated with, for example, an El Niño event. In average conditions like 1995/1996, about 0.6 PgC yr^{-1} are released to the atmosphere, which is slightly lower than the in situ and satellite-derived estimates of 0.9 ± 0.6 PgC from *Chavez et al.* [1999]. In association with the strong El Niño event in 1997/1998 we find a reduction to 0.2 PgC yr^{-1}, which is in agreement with the observational evidence of 0.2 ± 0.14 PgC [*Chavez et al.*, 1999]. A comparison of the modeled

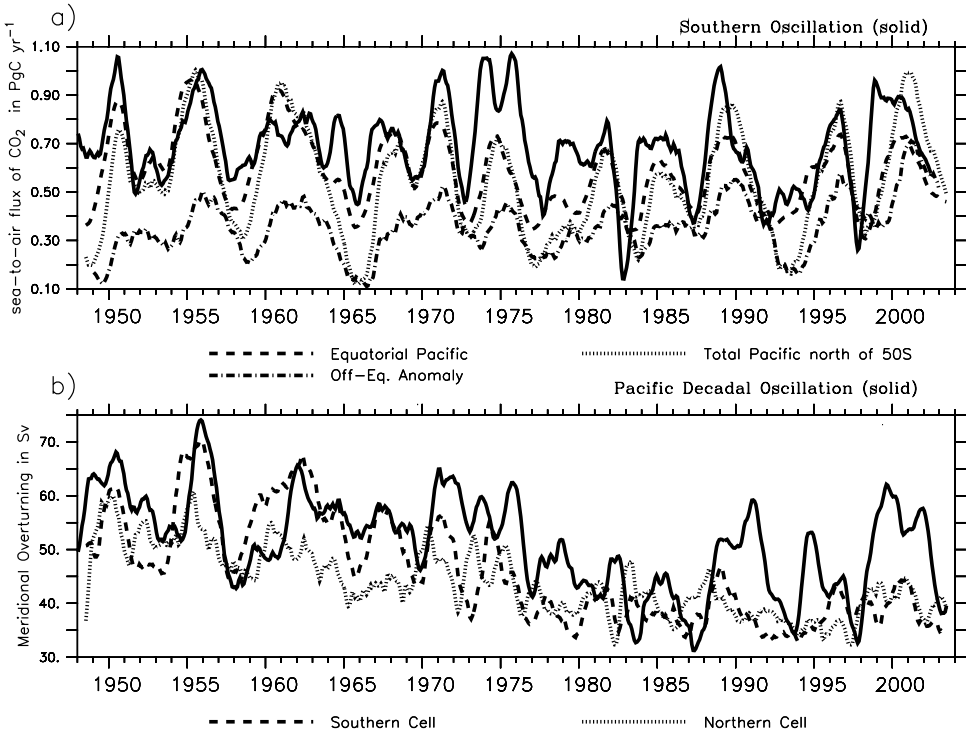

Figure 8. (a) Sea-to-air CO_2 fluxes of the control run (smoothed with a 12-month running mean) of the total Pacific and of equatorial Pacific from 10°N to 10°S and 80°W to 135°E. The Southern Oscillation Index is shown in blue. (b) Overturning of the southern and northern Equatorial Cell in the Pacific. The Pacific Decadal Oscillation Index is shown in blue. See color version of this figure at back of this issue.

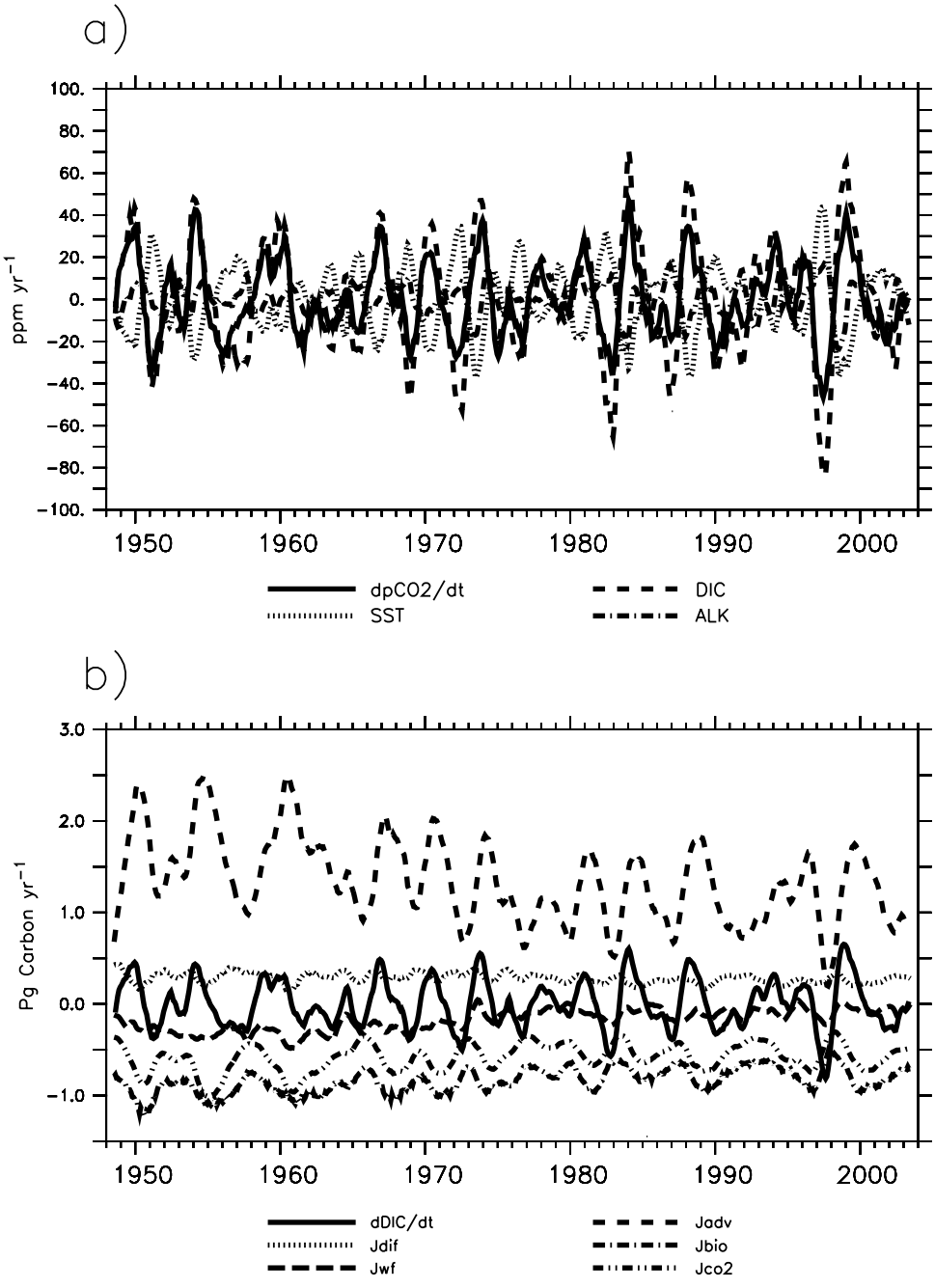

Figure 9. (a) Component analysis for the terms of equation (3) in the surface box of the equatorial Pacific from 10°S to 10°N and 80°W to 135°E. (b) Components of equation (4) for the upper 42 m of the same area. All fluxes are from the control run and smoothed with a 12-month running mean. See color version of this figure at back of this issue.

CO_2 flux with an extensive data compilation by *Feely et al.* [2002] for the equatorial Pacific (0°S to 5°S) is shown in Figure 10. The modeled fluxes and the variability agree reasonably well with the estimates from *Feely et al.* [2002] and *Chavez et al.* [1999].

[29] The absolute collapse of the upwelling in the first half and its recovery in the second half of 1998 is not completely reproduced by the model. This might be due to the coarse resolution of the model and to deficiencies in the NCEP/NCAR reanalysis over the tropical Pacific region. For example, *Chen* [2003] has evaluated four wind products, including the NCEP/NCAR reanalysis and the new Florida State University (FSU) subjective analysis, suggesting that the single largest discrepancy in wind stress are detected after the 1997/1998 El Niño. In the FSU analysis a strong and persistent westerly wind anomaly exists, but these changes are not reproduced by the NCEP/NCAR reanalysis. Also, the FSU analysis produces a stronger easterly anomaly

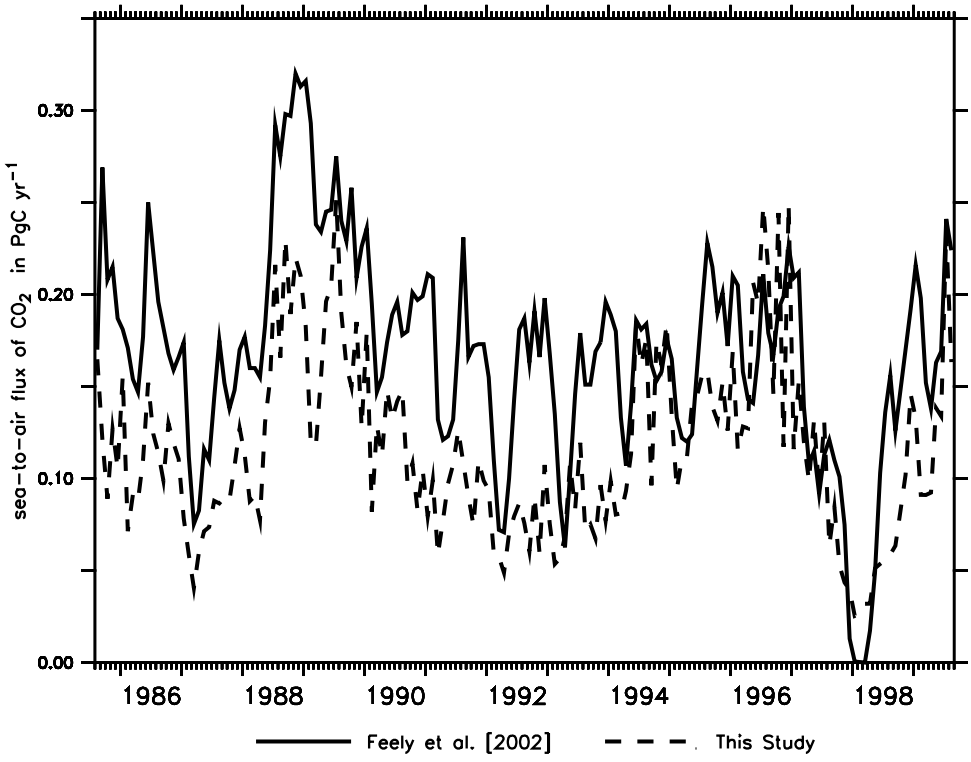

Figure 10. CO_2 flux estimate from *Feely et al.* [2002] for the equatorial Pacific from 0° to 5°S and the simulated CO_2 flux from the anthropogenic run.

in wind stress in the month preceding the 1997/1998 El Niño.

[30] In 1975–1977, there is regime shift [*Trenberth and Hurrell*, 1994] that can be seen in the Pacific Decadal Oscillation Index. It also is inherent in the NCEP/NCAR reanalysis (Figure 8). The interannual flux variability in the equatorial Pacific changes from ±0.33 PgC yr^{-1} (1948 to 1976) to ±0.27 PgC yr^{-1} (1977 to 2003). The wind-driven meridional overturning circulation is a good measure for the upwelling in the equatorial Pacific. The meridional overturning of the both equatorial cells in the Pacific changes from 100 ± 11 Sv to 77 ± 5 Sv. In the model, this is not an abrupt process, rather, a slowdown that starts in the mid 1960s and stabilizes at the beginning of the 1980s. This goes along with a reduction of the mean outgasing of CO_2 from 0.70 PgC yr^{-1} to 0.58 PgC yr^{-1}. This simulated slowdown of the overturning circulation by about 25% is in agreement with observational evidence [*McPhaden and Zhang*, 2002]. In a followup to this paper, *McPhaden and Zhang* [2004] report indications, from recent observations, that the shallow meridional overturning circulation in the tropical Pacific Ocean has rebounded since 1998. Our model shows an increase since 1998, but does not support a considerable rebound. The decrease of the interannual flux variability is restricted to the equatorial Pacific. Figure 8 shows that variability in the off-equatorial Pacific and in the total Pacific is almost constant over the full period. CO_2 fluxes in the off-equatorial and in the equatorial regions are more in phase during the second half of the 56-year period. Also, the frequency of the variability, as shown by the rate of change of the components $\frac{d\mathrm{DIC}}{dt}$ and $\frac{dpCO_2}{dt}$ in Figure 9, is larger during the second half.

4.2. Southern Ocean

[31] The global display of the standard deviations (2σ) in Figure 2b shows the highest interannual variability in the region from 40°S to 60°S (±0.1 PgC yr^{-1} with the trend subtracted). The seasonal cycle of pCO_2 in the Southern Ocean is controlled by biological production in summer and deep mixing in winter. An important factor determining the air-sea CO_2 flux is the mixed layer depth, which is related to the buoyancy fluxes and the wind stress.

[32] In the CR experiment, the CO_2 flux from 40°S to 60°S has a trend of 0.005 PgC yr^{-1} per year. The trend is caused by increasing wind speed over the Southern Ocean and is highly correlated to the Antarctic Oscillation (AAO) [*Thompson and Solomon*, 2002]. Increasing wind stress leads to higher advection and diffusion which bring DIC-rich deeper waters to the surface. Figure 11 shows the terms for advection and diffusion (J_{adv} and J_{dif} from equation (4)), the subsequent rise of CO_2 partial pressure, and their correlation with the AAO. CO_2 flux and pCO_2 rise linearly to each other. This implies that the flux is generated by the inner oceanic processes; the larger gas transfer coefficient only plays a minor role. The uptake of anthropogenic CO_2 is also increasing, because anthropogenic CO_2 penetrates faster into the deeper layers owing to enhanced ventilation.

[33] Recent estimates from atmospheric inversions [*Roy et al.*, 2003; *Rödenbeck et al.*, 2003; *Gurney et al.*, 2002] show a flux of about −1 PgC yr^{-1} for the Southern Hemisphere,

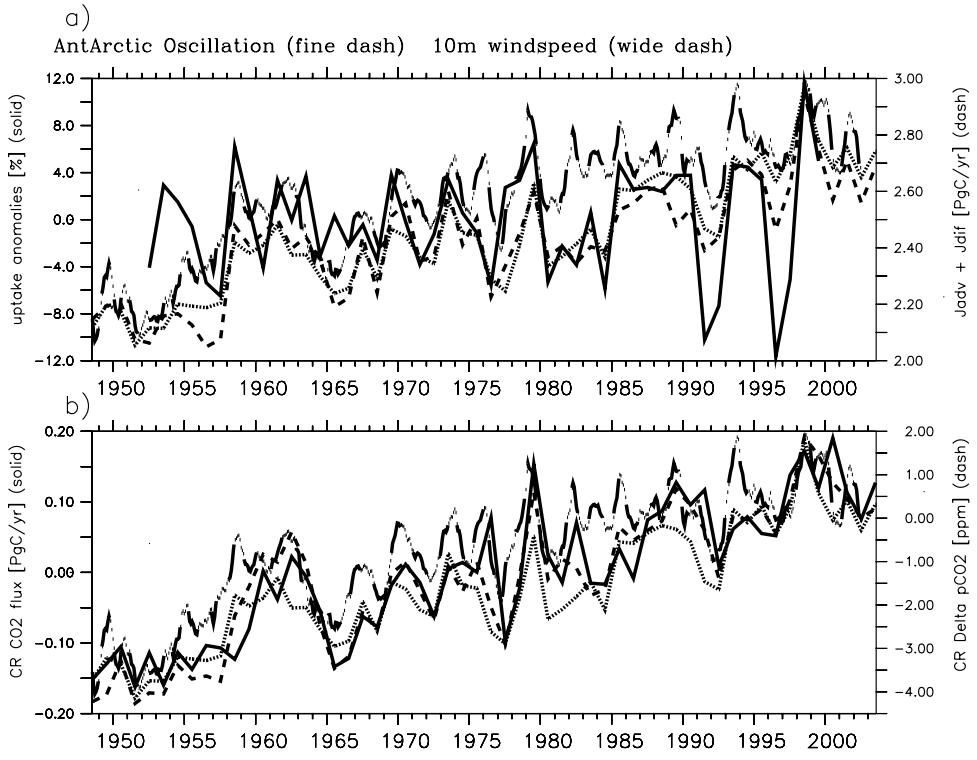

Figure 11. Yearly means for the Southern Ocean from 40°S to 60°S. In blue is the Antarctic Oscillation Index, and in green is the 10-m wind speed from the NCEP reanalysis. (a) Anomaly in the uptake of anthropogenic CO_2 (AR experiment) and carbon transported into the upper 42 m by advection and diffusion (components of equation (4). (b) CO_2 flux and ΔpCO_2 from the control run (CR). See color version of this figure at back of this issue.

but vary considerably in the partitioning between the Southern Ocean and the midlatitudes (Table 4). The model shows the highest influx south of 50°S (Figure 5a), which is in agreement with *Gurney et al.* [2002] and in disagreement with *Rödenbeck et al.* [2003] (Table 4).

[34] Estimates based on interpolated pCO_2 measurements show a high CO_2 flux into the ocean in the Southern Hemisphere [*Takahashi et al.*, 2002]. *Metzl et al.* [1999] extrapolate a flux of about -1 PgC yr^{-1} for the sub-Antarctic zone from about 40°S–50°S alone. Estimates from atmospheric inversions and findings from this study indicate a smaller CO_2 influx. The remote Southern Ocean has a sparse data coverage, particularly in winter, so it is necessary to extrapolate the regional estimates over the seasonal cycle, which may explain the discrepancies. The model has a strong seasonal cycle with a large CO_2 influx in December and January and outgasing from February to May. The CO_2 fluxes calculated from the climatology from *Takahashi et al.* [2002] show a weak seasonal cycle with a minimum influx of CO_2 in June/July. Atmospheric inversions by *Roy et al.* [2003] and *Gurney et al.* [2004] indicate a stronger cycle, *Roy et al.* [2003] even find a weak outgasing for February to May, but their seasonal cycle is less pronounced than predicted by the model (Figure 12).

[35] The uptake rates of anthropogenic carbon for 1980–1989 and for 1990–1999 in the Southern Ocean are almost comparable to the uptake rates in the deep water formation areas in the North Atlantic. The model shows the highest uptake rates in the Southern Ocean from 50°S to 70°S (Figure 5a), while the highest storage occurs out of the Southern Ocean north of 50°S (Figure 5b). Half of the anthropogenic CO_2 taken up by the Southern Ocean is transported northward into the subtropical convergence (Table 5), which is supported by the study of *Caldeira and Duffy* [2000].

[36] The estimated distribution of anthropogenic CO_2 by *Lee et al.* [2003] and *Sabine et al.* [2002, 1999] are generally in good agreement with the model. These studies indicate relatively little storage of anthropogenic CO_2 in the Southern Ocean and high storage in the subtropical convergence. The model estimates compare well with the inventories for the Pacific and the Indian Ocean given by *Sabine et al.* [2002, 1999]. In the Atlantic, model estimates are lower than results from *Lee et al.* [2003]. An interesting exception is the Weddell Sea between 60°E and 20°W, where deep convection in coherence with the formation of sea ice is entraining anthropogenic CO_2 into the deep Southern Ocean (Figure 5b). This study predicts an inventory of 1.3 Pg anthropogenic CO_2 in the Atlantic from 70°S to 60°S by 1995, which is 1 PgC more than the estimates by *Lee et al.* [2003].

4.3. North Atlantic, Greenland, Iceland, Norwegian, and Labrador Seas

[37] It is generally accepted that the North Atlantic is a strong sink for CO_2. The modeled CO_2 flux and variability

Table 4. Sea-to-air CO_2 Fluxes Partitioned Between the Southern Ocean and the Midlatitudes of the Southern Hemisphere

	Year(s)	50°S–90°S	14°S–50°S	Total
Roy et al. [2003]	1991–1997	−0.3	−0.7	−1.0
Rödenbeck et al. [2003]	1990–1999	0.0 ± 0.1	−1.0 ± 4.7	−1.0
Gurney et al. [2002]	1992–1996	−0.5	−0.4	−0.9
Gurney et al. [2004][a]	1992–1996	−0.55 ± 0.33	+0.07 ± 0.54	−0.48
Takahashi et al. [2002]	1995	−0.35	−1.16	−1.51
This study	1990–1999	−0.56	−0.45	−1.1

[a]The main difference from *Gurney et al.* [2002] is the removal of the Darwin CO_2 observing station from the analysis.

Table 5. Uptake and Storage of Anthropogenic CO_2 in the Southern Ocean (SO) and the Midlatitudes of the Southern Hemisphere in PgC

	14°S–50°S	SO 50°S–90°S	SO Indian	SO Atlantic	SO Pacific
Total storage (1980–1989)	6.1	1.9	0.5	0.5	0.9
Total uptake (1980–1989)	4.9	3.7	1.1	0.8	1.8
Total storage (1990–1999)	7.3	2.1	0.6	0.6	1.0
Total uptake (1990–1999)	5.8	4.6	1.5	1.1	2.0

of the North Atlantic north of 50 N is -0.31 ± 0.04 PgC yr^{-1} in the CR and -0.41 ± 0.05 for 1990–1999 in the AR experiment.

[38] The model produces a deep penetration of anthropogenic CO_2 in the high northern latitudes of the Atlantic. This is in agreement with $\Delta C^{\star}$ technique estimates by *Lee et al.* [2003] and *Gruber* [1998] and CFC data estimates from *McNeil et al.* [2003]. Most important are the deep water formation areas north of 50°N, the Labrador, Greenland, Iceland, and Norwegian (GIN) seas. The high inventories of anthropogenic CO_2 in the high latitudes of the North Atlantic reach deeper than anywhere else in the world. However, *Völker et al.* [2002] raised the question of whether this implies that the flux of carbon from the atmosphere into the North Atlantic has increased over its preindustrial value. Uptake and storage of anthropogenic CO_2 in the North Atlantic are summarized in Table 6. Similar to the Southern Hemisphere, the accumulation of anthropogenic CO_2 in the midlatitudes is higher than the oceanic uptake of anthropogenic CO_2 by air-sea gas exchange. The Arctic Ocean is fed by waters from the Bering Strait and the West Spitsbergen Current which are well equilibrated with the atmospheric CO_2 concentrations. The storage in the Arctic Ocean is estimated to be 4 times higher than the uptake by the air-sea gas exchange. In areas of North Atlantic Deep Water formation, for example, GIN and Labrador seas, intense surface cooling and deep winter convection carry the anthropogenic CO_2 signal down to the bottom of the ocean. Accumulation of anthropogenic CO_2 in the GIN Sea is

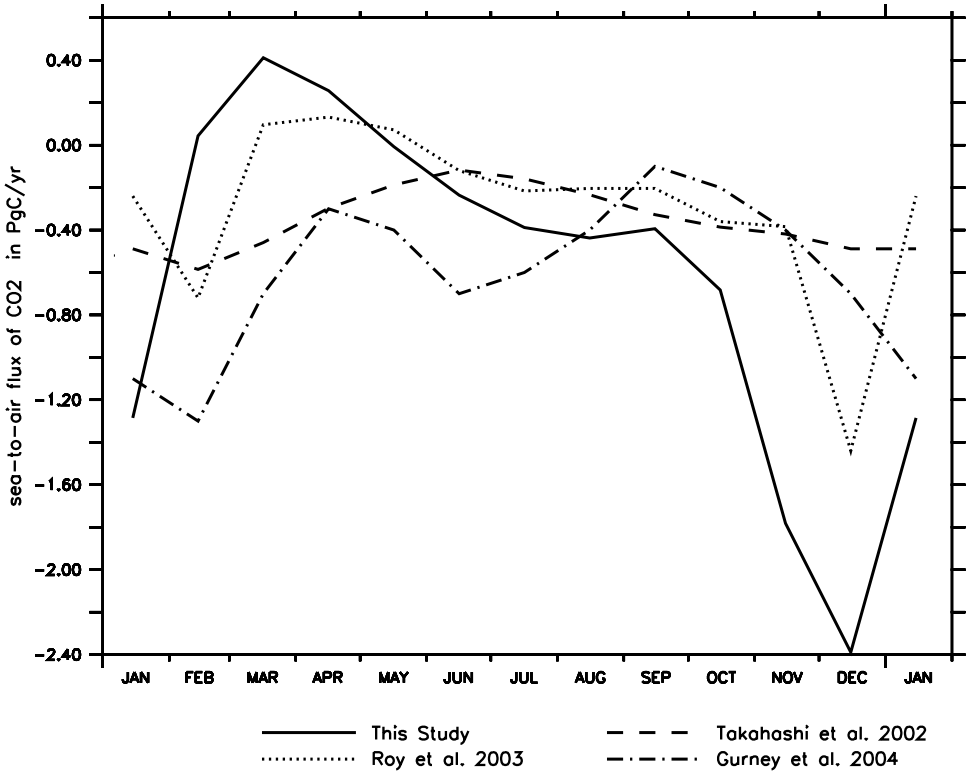

Figure 12. Seasonal cycle of CO_2 fluxes in the Southern Ocean south of 50°S averaged from 1990 to 1999.

Table 6. Uptake and Storage of Anthropogenic CO_2 in the North Atlantic and the Northern High Latitudes in PgC

	50°N–14°N	70°N–50°N[a]	GIN Sea	Labrador	Arctic
Total storage (1980–1989)	2.07	0.57	0.24	0.15	0.30
Total uptake (1980–1989)	1.06	0.46	0.31	0.12	0.07
Total storage (1990–1999)	2.52	0.60	0.17	0.16	0.41
Total uptake (1990–1999)	1.17	0.59	0.35	0.14	0.10

[a]Excluding the GIN and Labrador seas.

lower than the uptake of anthropogenic CO_2 by air-sea gas exchange. Most of the water masses transported into the GIN Sea originate in the North Atlantic Current and are not fully equilibrated with the atmospheric CO_2 concentrations, and a significant fraction of the anthropogenic CO_2 taken up by air-sea gas exchange is transported out of the GIN Sea with the East Greenland Current and the Denmark Strait overflow. In the Labrador Sea and the remaining part of the North Atlantic from 70°N–50°N (excluding the GIN and Labrador Seas) the in- and out-flows of anthropogenic CO_2 are roughly in balance. Highest rates of anthropogenic CO_2 uptake are simulated in deep convection areas near Greenland. This uptake is reduced by a rising buffer factor, causing only a small increase from 1980–1989 to 1990–1999 (Table 6).

[39] Figure 2b shows areas of high interannual CO_2 flux variability in the high northern latitudes. In the Arctic Ocean, parts of the Labrador Sea, and along the coast of Greenland the sea-ice cover strongly influences the interannual variability. However, the areas are small and the variations are not in phase with each other, resulting in a relatively low interannual variability of the entire North Atlantic. On decadal timescales, these regions are characterized by a stationary behavior which is in contrast to the Southern Ocean and the equatorial Pacific. The Southern Ocean and the North Atlantic regions have a large seasonal cycle compared to the relatively low variability on interannual scales.

[40] An important index to analyze the variability in the North Atlantic, the GIN, and Labrador Seas is the North Atlantic Oscillation (NAO) [*Hurrell et al.*, 2003]. The NAO is defined as the difference between the subtropical high-pressure systems near the Azores and the subpolar lows near Iceland. Figure 13 shows the correlation of wintertime NAO with wintertime MLD and average CO_2 fluxes from the CR. As analyzed by *Cullen et al.* [2001], a strong pressure difference (NAO high) correlates with low MLD anomalies in the subtropics and high MLD anomalies in the subpolar gyre. The CO_2 flux is not always correlated with the MLD, and the total flux shows almost no correlation ($r = 0.2$) with the NAO Index. This results from the competing influences of the components of equation (3) (Figure 13). In contrast, the interannual variations in the uptake of anthropogenic CO_2 are mostly controlled by changes in the mixed layer depth (MLD). Anthropogenic carbon is entrained deep into the ocean, and older waters with low anthropogenic concentrations are mixed to the surface. Therefore, north of 50°N, the simulated oceanic uptake of anthropogenic CO_2 is correlated with the winter NAO index and anti-correlated in the subtropical gyre.

[41] The connection between key parameters and the CO_2 flux and uptake in the GIN Sea and the Labrador Sea is shown in Figures 14 and 15. Uptake of anthropogenic CO_2 in the Labrador Sea is tightly connected to the MLD, which itself is correlated to the NAO index, but also responds to the wind speed (Figure 15a). The 10-m wind speed in the Labrador Sea has almost no correlation with the NAO index. In the GIN Sea, the MLD does not correlate to the NAO index, but the 10-m wind speed does. Like in the Labrador Sea, the uptake depends on the wind and the MLD (Figure 14a). In both regions, the GIN Sea and the Labrador Sea, the average CO_2 flux is negative. The CO_2 in-flux in the CR is tightly connected with the 10-m wind speed. In contrast to the Southern Ocean (Figure 11b), in both regions the CO_2 flux does not directly follow the ΔpCO_2. ΔpCO_2 depends on the mixing and also reacts to the CO_2 flux. A high flux into the ocean causes a decrease of the absolute value of the negative CO_2 partial pressure difference.

5. Conclusion and Discussion

[42] We have used a fully prognostic biogeochemical global ocean circulation model, forced with surface fluxes computed from NCEP/NCAR reanalysis data for the period 1948–2003. The natural variability and the trends are analyzed in a control run with preindustrial atmospheric CO_2 concentrations. In addition, the response of the system to anthropogenic atmospheric CO_2 concentrations has been tested. The total interannual variability of the model is ± 0.50 PgC yr^{-1} (2σ). This is within the range of previous ocean model studies [*Le Quéré et al.*, 2000; *Obata and Kitamura*, 2003; *McKinley et al.*, 2004] and recent atmospheric inversions [*Rödenbeck et al.*, 2003]. The CO_2 flux is -1.49 PgC yr^{-1} for 1980–1989 and -1.74 PgC yr^{-1} for 1990–1999. Our simulated fluxes agree well with flux estimates from atmospheric inversions [*Rödenbeck et al.*, 2003; *Gurney et al.*, 2002] (Table 2).

[43] We define the uptake of anthropogenic CO_2 as the difference between the CO_2 fluxes of the anthropogenic run and the control run. The uptake of anthropogenic CO_2 is 1.65 PgC yr^{-1} for 1980–1989 and 1.91 PgC yr^{-1} for 1990–1999, with an accumulation of about 105 Pg of anthropogenic carbon by 1995. The inventory estimate is compatible with results from chlorofluorocarbon [*McNeil et al.*, 2003] and from ΔC technique estimates [*Lee et al.*, 2003; *Sabine et al.*, 2002, 1999].

[44] Decadal variability is dominated by the regime shift in the Pacific in the middle of the simulation period and the increase of the CO_2 fluxes in the Southern Ocean over the full 56-year simulation period. During the regime shift in 1975–1977 the modeled interannual variability in the equatorial Pacific changes from ± 0.32 PgC yr^{-1} to ± 0.23 PgC yr^{-1} and the mean outgasing of CO_2 decreases from 0.70 PgC yr^{-1} to 0.58 PgC yr^{-1}.

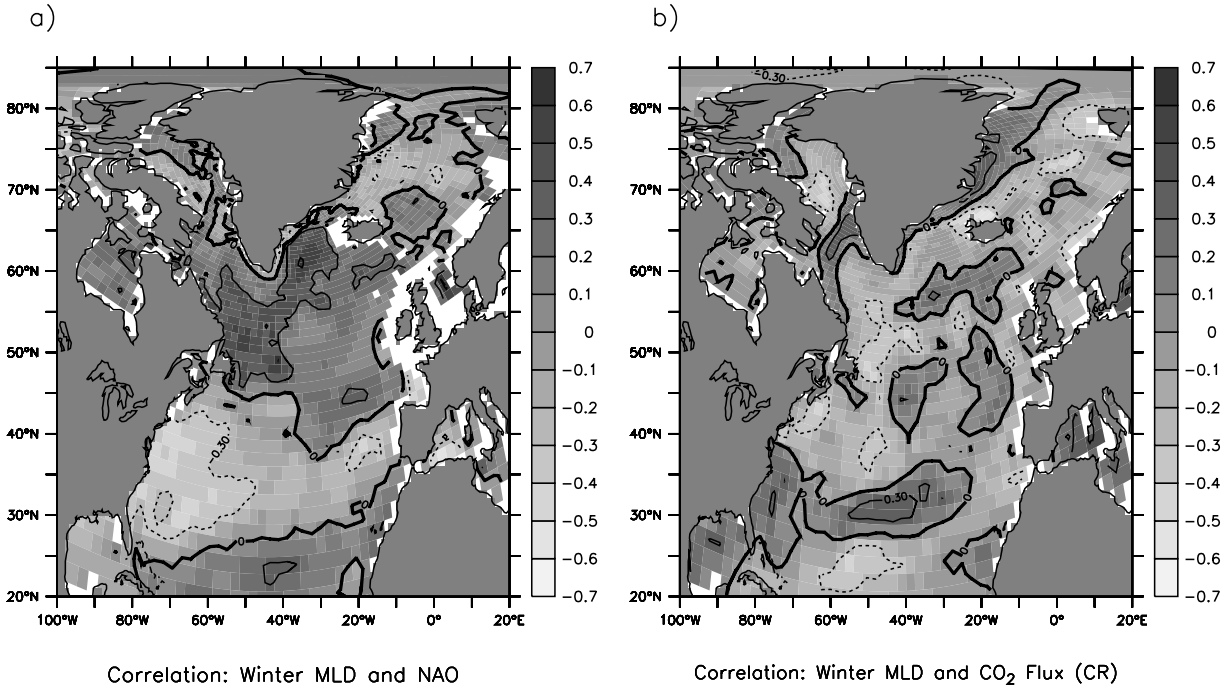

Figure 13. Correlation of the wintertime North Atlantic Oscillation (NAO) with (a) winter mixed layer depth and (b) mean sea-to-air CO_2 flux anomalies from the control run (CR). See color version of this figure at back of this issue.

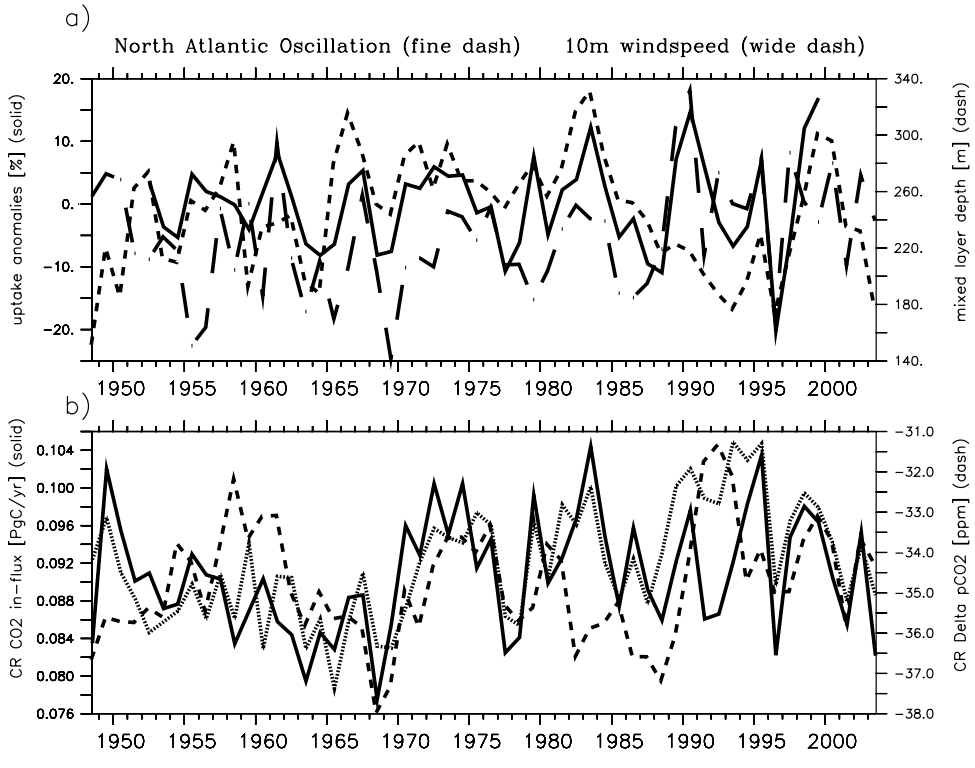

Figure 14. Yearly means for the Greenland, Iceland, and Norwegian seas. In blue is the North Atlantic Oscillation Index, and in green is the 10-m wind speed from the NCEP reanalysis. (a) Anomaly in the uptake of anthropogenic CO_2 (AR experiment) and the average mixed layer depth. (b) CO_2 in-flux and ΔpCO_2 from the control run (CR). See color version of this figure at back of this issue.

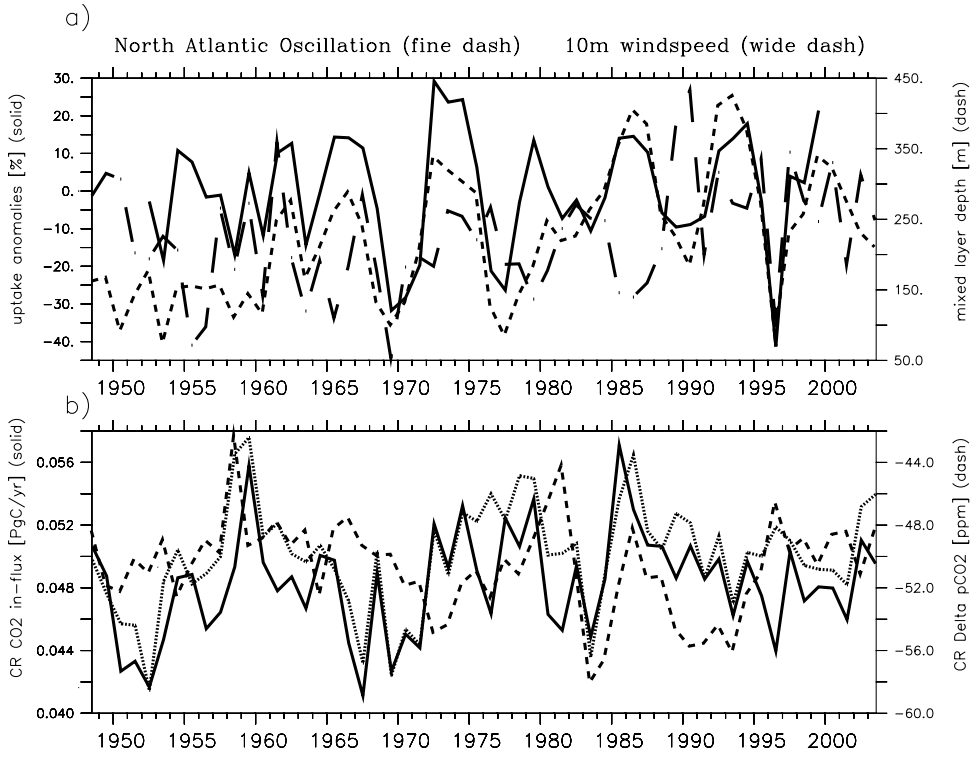

Figure 15. Yearly means for the Labrador Sea. In blue is the North Atlantic Oscillation Index, and in green is the 10-m wind speed from the NCEP reanalysis. (a) Anomaly in the uptake of anthropogenic CO_2 (AR experiment) and the average mixed layer depth. (b) CO_2 in-flux and ΔpCO_2 from the control run (CR). See color version of this figure at back of this issue.

[45] The regime shift in the Pacific reduces the outgasing of CO_2 in the equatorial Pacific during the second half of the 56-year period. However, the global sea-to-air CO_2 flux in the CR increases by 0.006 PgC yr^{-1} per year on average. The reason for this trend is a strengthening of the wind over the Southern Hemisphere which leads to higher mixing. It is interesting to note that the major factor for the increasing CO_2 fluxes is the rising ΔpCO_2 due to the increase in DIC and not the larger gas transfer coefficient. Because of this trend, the global CO_2 flux in the anthropogenic experiment is about 0.18 PgC yr^{-1} smaller (from 1980 to 2003) than the computed uptake of anthropogenic CO_2. Trends in a forced system also depend on the initial conditions. It is an important aspect of this study that the model was integrated to a cyclostationary state with a NCEP/NCAR forcing set detrended with respect to 1948. The trends therefore reflect changes with respect to a mean state, which is consistent with the beginning of the forcing period.

[46] Interannual variability and trends in the model are caused by changes in ocean circulation and mixing, acting on biogeochemical tracers such as DIC. Nevertheless, this study underlines that the marine biology has a significant influence on the interannual variability by shaping the distribution of the biogeochemical tracers. An example is the effect the iron limitation has in the equatorial Pacific. The limited production changes the distribution of dissolved inorganic carbon (DIC) and reduces the interannual CO_2 flux variability.

[47] **Acknowledgments.** We thank Iris Kriest for valuable assistance with the biological model, Angelika Heil, Silvia Kloster, Katharina Six, and Johann Jungclaus for helpful comments on the manuscript, and Taro Takahashi and Richard Feely for the data in Figures 3 and 10. This work has been funded by the EU grant EVK2-CT-2001-00134 "Northern Ocean-Atmosphere Carbon Exchange Study" and NASA NAG5-11245 "Carbon Cycle Science."

References

Aumont, O., E. Maier-Reimer, S. Blain, and P. Monfray (2003), An ecosystem model of the global ocean including Fe, Si, P colimitations, *Global Biogeochem. Cycles*, *17*(2), 1060, doi:10.1029/2001GB001745.

Bopp, L., C. Le Quéré, M. Heimann, A. C. Manning, and P. Monfray (2002), Climate-induced oceanic oxygen fluxes: Implications for the contemporary carbon budget, *Global Biogeochem. Cycles*, *16*(2), 1022, doi:10.1029/2001GB001445.

Caldeira, K., and P. B. Duffy (2000), The role of the Southern Ocean in uptake and storage of anthropogenic carbon dioxide, *Science*, *287*, 620–622.

Chavez, F. P., P. G. Strutton, G. E. Friederich, R. A. Feely, G. C. Feldman, D. G. Foley, and M. J. McPhaden (1999), Biological and chemical response of the equatorial Pacifc Ocean to the 1997/98 El Niño, *Science*, *286, 2126–2131.*

Chen, D. (2003), A comparison of wind products in the context of ENSO prediction, *Geophys. Res. Lett.*, *30*(3), 1107, doi:10.1029/2002GL016121.

Coale, K. H., et al. (1996), A massive phytoplankton bloom induced by an ecosystem-scale iron fertilization experiment in the equatorial Pacific Ocean, *Nature*, *383*, 495–501.

Conkright, M., S. Levitus, T. O'Brien, T. Boyer, J. Antonov, and C. Stephens (1998), *World Ocean Atlas 1998 Data Set Documentation* [CD-ROM], *Tech. Rep. 15*, 16 pp., Natl. Oceanic and Atmos. Admin., Silver Spring, Md.

Cullen, H. M., R. D. D'Arrigo, and E. R. Cook (2001), Multiproxy reconstruction of the North Atlantic Oscillation, *Paleoceanography*, *16*(1), 27–39.

Enting, I. G., T. M. L. Wigley, and M. Heimann (1994), Future emissions and concentrations of carbon dioxide: Key ocean/atmosphere/land analysis, *Tech. Pap. 31*, Div. of Atmos. Res., Commonw. Sci. and Ind. Res. Org., Melbourne, Victoria, Australia.

Feely, R. A., R. Wanninkhof, T. Takahashi, and P. Tans (1999), Influence of El Niño on the equatorial Pacific contribution to atmospheric CO_2 accumulation, *Nature*, *398*, 597–601.

Feely, R. A., et al. (2002), Seasonal and interannual variability of CO_2 in the equatorial Pacific, *Deep Sea Res., Part II*, *49*, 2443–2469.

Francey, R. J., P. P. Tans, C. E. Allison, I. G. Enting, J. W. C. White, and M. Trolier (1995), Changes in oceanic and terrestrial carbon uptake since 1982, *Nature*, *373*, 326–330.

Gent, P. R., J. Willebrand, T. McDougall, and J. C. McWilliams (1995), Parameterizing eddy-induced tracer transport in ocean circulation models, *J. Phys. Oceanogr.*, *25*, 463–474.

Gruber, N. (1998), Anthropogenic CO_2 in the Atlantic Ocean, *Global Biogeochem. Cycles*, *12*(1), 165–192.

Gruber, N., and C. D. Keeling (2001), An improved estimate of the isotopic air-sea disequilibrium of CO_2: Implications for the oceanic uptake of anthropogenic CO_2, *Geophys. Res. Lett.*, *28*, 555–558.

Gruber, N., J. L. Sarmiento, and T. F. Stocker (1996), An improved method for detecting anthropogenic CO_2 in the oceans, *Global Biogeochem. Cycles*, *10*(4), 809–837.

Gurney, K. R., et al. (2002), Towards robust regional estimates of CO_2 sources and sinks using atmospheric transport models, *Nature*, *415*, 626–630.

Gurney, K. R., et al. (2004), Transcom 3 inversion intercomparison: Model mean results for the estimation of seasonal carbon sources and sinks, *Global Biogeochem. Cycles*, *18*, GB1010, doi:10.1029/2003GB002111.

Heimann, M., and E. Maier-Reimer (1996), On the relations between the oceanic uptake of CO_2 and its carbon isotopes, *Global Biogeochem. Cycles*, *10*(1), 89–110.

Heinze, C., A. Hupe, E. Maier-Reimer, N. Dittert, and O. Ragueneau (2003), Sensitivity of the marine biospheric Si cycle for biogeochemical parameter variations, *Global Biogeochem. Cycles*, *17*(3), 1086, doi:10.1029/2002GB001943.

Hibler, W. D. (1979), A dynamic thermodynamic sea ice model, *J. Phys. Oceanogr.*, *9*, 815–846.

Hurrell, J. W., Y. Kushnir, G. Ottersen, and M. Visbeck (Eds.) (2003), *The North Atlantic Oscillation: Climate Significance and Environmental Impact*, *Geophys. Monogr. Ser.*, vol. 134, 279 pp., AGU, Washington, D. C.

Intergovernmental Panel on Climate Change (2001), *Climate Change 2001: The Scientific Basis, Contribution of Working Group I to the Third Assessment Report of the Intergovernmental Panel on Climate Change (IPCC)*, edited by J. T. Houghton et al., Cambridge Univ. Press, New York.

Johnson, K. S., R. M. Gordon, and K. H. Coale (1997), What controls dissolved iron concentrations in the world ocean?, *Mar. Chem.*, *57*, 137–161.

Joos, F., R. Meyer, M. Bruno, and M. Leuenberger (1999), The variability in the carbon sinks as reconstructed for the last 1000 years, *Geophys. Res. Lett.*, *26*, 1437–1440.

Kalnay, E., et al. (1996), The NCEP/NCAR 40-year reanalysis project, *Bull. Am. Meteorol. Soc.*, *77*(3), 437–470.

Keeling, C. D., and T. P. Whorf (2002), Atmospheric CO_2 records from sites in the SIO air sampling network, in *Trends: A Compendium of Data on Global Change*, pp. 1–28, Carbon Dioxide Inf. Anal. Cent., Oak Ridge Natl. Lab., U.S. Dep. of Energy, Oak Ridge, Tenn.

Keeling, C. D., T. P. Whorf, M. Wahlen, and J. van der Plicht (1995), Interannual extremes in the rate of rise of atmospheric carbon dioxide since 1980, *Nature*, *375*, 666–670.

Keeling, R. F., and S. R. Shertz (1992), Seasonal and interannual variations in atmospheric oxygen and implications for the global carbon cycle, *Nature*, *358*, 723–727.

Key, R. M., A. Kozyr, C. L. Sabine, K. Lee, R. Wanninkhof, J. Bullister, R. A. Feely, F. Millero, C. Mordy, and T.-H. Peng (2004), A global ocean carbon climatology: Results from Global Data Analysis Project (GLODAP), *Global Biogeochem. Cycles*, *18*, GB4031, doi:10.1029/2004GB002247.

Lee, K., R. Wanninkhof, T. Takahashi, S. C. Doney, and R. A. Feely (1998), Low interannual variability in recent oceanic uptake of atmospheric cabon dioxide, *Nature*, *396*, 155–158.

Lee, K., et al. (2003), An updated anthropogenic CO_2 inventory in the Atlantic Ocean, *Global Biogeochem. Cycles*, *17*(4), 1116, doi:10.1029/2003GB002067.

Le Quéré, C., J. C. Orr, P. Monfray, and O. Aumont (2000), Interannual variability of the oceanic sink of CO_2 from 1979 through 1997, *Global Biogeochem. Cycles*, *14*(4), 1247–1265.

Maier-Reimer, E. (1993), Geochemical cycles in an ocean general circulation model: Preindustrial tracer distribution, *Global Biogeochem. Cycles*, *7*(3), 645–677.

Maier-Reimer, E., and I. Kriest (2005), The marine biogeochemical model HAMOCC5, report, Max-Planck-Institute for Meteorology, Hamburg, Germany, in press. (Available at http://www.mpimet.mpg.de)

Marsland, S. J., H. Haak, J. H. Jungclaus, M. Latif, and F. Roeske (2003), The Max-Planck-Institute global ocean/sea ice model with orthogonal curvilinear coordinates, *Ocean Modell.*, *5*(2), 91–127.

Matsumoto, K., et al. (2004), Evaluation of ocean carbon cycle models with data-based metrics, *Geophys. Res. Lett.*, *31*, L07303, doi:10.1029/2003GL018970.

McKinley, A. G., M. J. Follows, and J. Marshall (2004), Mechanisms of air-sea CO_2 flux variability in the equatorial Pacific and the North Atlantic, *Global Biogeochem. Cycles*, *18*, GB2011, doi:10.1029/2003GB002179.

McNeil, I. B., R. J. Matear, R. M. Key, J. L. Bullister, and J. L. Sarmiento (2003), Anthropogenic CO_2 uptake by the ocean based on the global chlorofluorocarbon data set, *Science*, *299*, 235–239.

McPhaden, M. J., and D. Zhang (2002), Slowdown of the meridional overturning circulation in the upper Pacific Ocean, *Nature*, *415*, 603–608.

McPhaden, M. J., and D. Zhang (2004), Pacific Ocean circulation rebounds, *Geophys. Res. Lett.*, *31*, L18301, doi:10.1029/2004GL020727.

Metzl, N., B. Tilbrook, and A. Poisson (1999), The annual fCO_2 cycle and the air-sea CO_2 flux in the sub-Antarctic Ocean, *Tellus, Ser. B*, *51*, 849–861.

Obata, A., and Y. Kitamura (2003), Interannual variability of sea-air exchange of CO_2 from 1961 to 1998 with a global ocean circulation biogeochemistry model, *J. Geophys. Res.*, *108*(C11), 3337, doi:10.1029/2001JC001088.

Rayner, P., I. Enting, R. J. Francey, and R. Langenfelds (1999), Reconstructing the recent carbon cycle from atmospheric CO_2, $d^{13}C$ and N_2/O_2 observations, *Tellus, Ser. B*, *51*, 213–232.

Rödenbeck, C., S. Houweling, M. Gloor, and M. Heimann (2003), CO_2 flux history 1982–2001 inferred from atmospheric data using a global inversion of atmospheric transport, *Atmos. Chem. Phys.*, *3*, 1919–1964.

Roy, T., P. Rayner, R. Matear, and R. J. Francey (2003), Southern Hemisphere ocean CO_2 uptake: Reconciling atmospheric and oceanic estimates, *Tellus, Ser. B*, *55*, 701–710.

Sabine, C. L., R. M. Key, K. M. Johnson, F. J. Millero, A. Poisson, J. L. Sarmiento, D. W. R. Wallace, and C. D. Winn (1999), Anthropogenic CO_2 inventory of the Indian Ocean, *Global Biogeochem. Cycles*, *13*(1), 179–198.

Sabine, C. L., R. A. Feely, R. M. Key, J. L. Bullister, F. J. Millero, K. Lee, T.-H. Peng, B. Tilbrook, T. Ono, and C. S. Wong (2002), Distribution of anthropogenic CO_2 in the Pacific Ocean, *Global Biogeochem. Cycles*, *16*(4), 1083, doi:10.1029/2001GB001639.

Sabine, C. L., et al. (2004), The Oceanic sink for anthropogenic CO_2, *Science*, *305*, 367–371.

Six, K. D., and E. Maier-Reimer (1996), Effects of plankton dynamics on seasonal carbon fluxes in an ocean general circulation model, *Global Biogeochem. Cycles*, *10*(4), 559–583.

Sweby, P. K. (1984), High resolution schemes using flux limiters for hyperbolic conservation laws, *SIAM J. Numer. Anal.*, *21*(5), 995–1011.

Takahashi, T., J. Olafsson, J. G. Goddard, D. W. Chipman, and S. C. Sutherland (1993), Seasonal variation of CO_2 and nutrients in the high-latitude surface oceans: A comparative study, *Global Biogeochem. Cycles*, *7*(4), 843–878.

Takahashi, T., et al. (2002), Global sea-air CO_2 flux based on climatological surface ocean pCO_2, and seasonal biological and temperature effects, *Deep Sea Res., Part II*, *49*, 1601–1622.

Thompson, D. W. J., and S. Solomon (2002), Interpretation of recent Southern Hemisphere climate change, *Science*, *296*, 895–899.

Timmreck, C., and M. Schulz (2004), Significant dust simulation differences in nudged and climatological operation mode of the AGCM ECHAM, *J. Geophys. Res.*, *109*, D13202, doi:10.1029/2003JD004381.

Trenberth, K. E., and J. W. Hurrell (1994), Decadal atmosphere-ocean variations in the Pacific, *Clim. Dyn.*, *9*, 303–319.

Völker, C., D. W. R. Wallace, and D. A. Wolf-Gladrow (2002), On the role of heat fluxes in the uptake of anthropogenic carbon in the North Atlantic, *Global Biogeochem. Cycles*, *16*(4), 1138, doi:10.1029/2002GB001897.

Wanninkhof, R. (1992), Relationship between wind speed and gas exchange over the ocean, *J. Geophys. Res.*, *97*, 7373–7382.

Winguth, A. M. E., M. Heimann, K. D. Kurz, E. Maier-Reimer, U. Mikolajewicz, and J. Segschneider (1994), El Niño-Southern Oscillation related fluctuations of the marine carbon cycle, *Global Biogeochem. Cycles*, *8*(1), 39–63.

Zeng, N., A. Mariotti, and P. Wetzel (2005), Terrestrial mechanisms of interannual CO_2 variability, *Global Biogeochem. Cycles*, *19*, GB1016, doi:10.1029/2004GB002273.

E. Maier-Reimer and P. Wetzel, Max Planck Institute for Meteorology, Bundesstrasse 53, D-20146 Hamburg, Germany. (patrick.wetzel@dkrz.de)

A. Winguth, Center for Climatic Research, University of Wisconsin-Madison, 1225 West Dayton Street, Madison, WI 53706, USA.

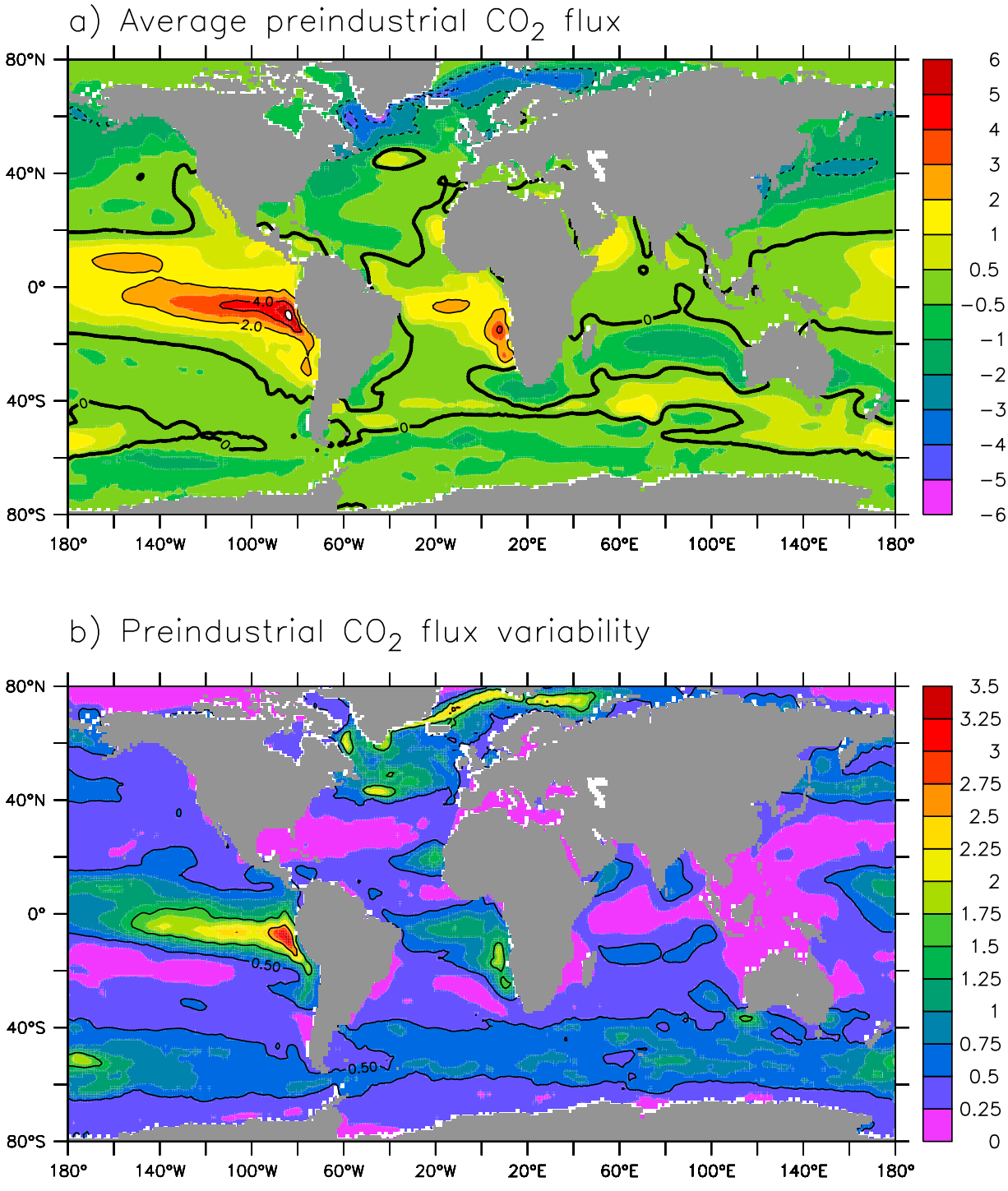

Figure 2. (a) Average CO_2 flux and (b) CO_2 2σ-variability of the control run in PgC yr^{-1}, simulated with MPIOM-HAMOCC5.

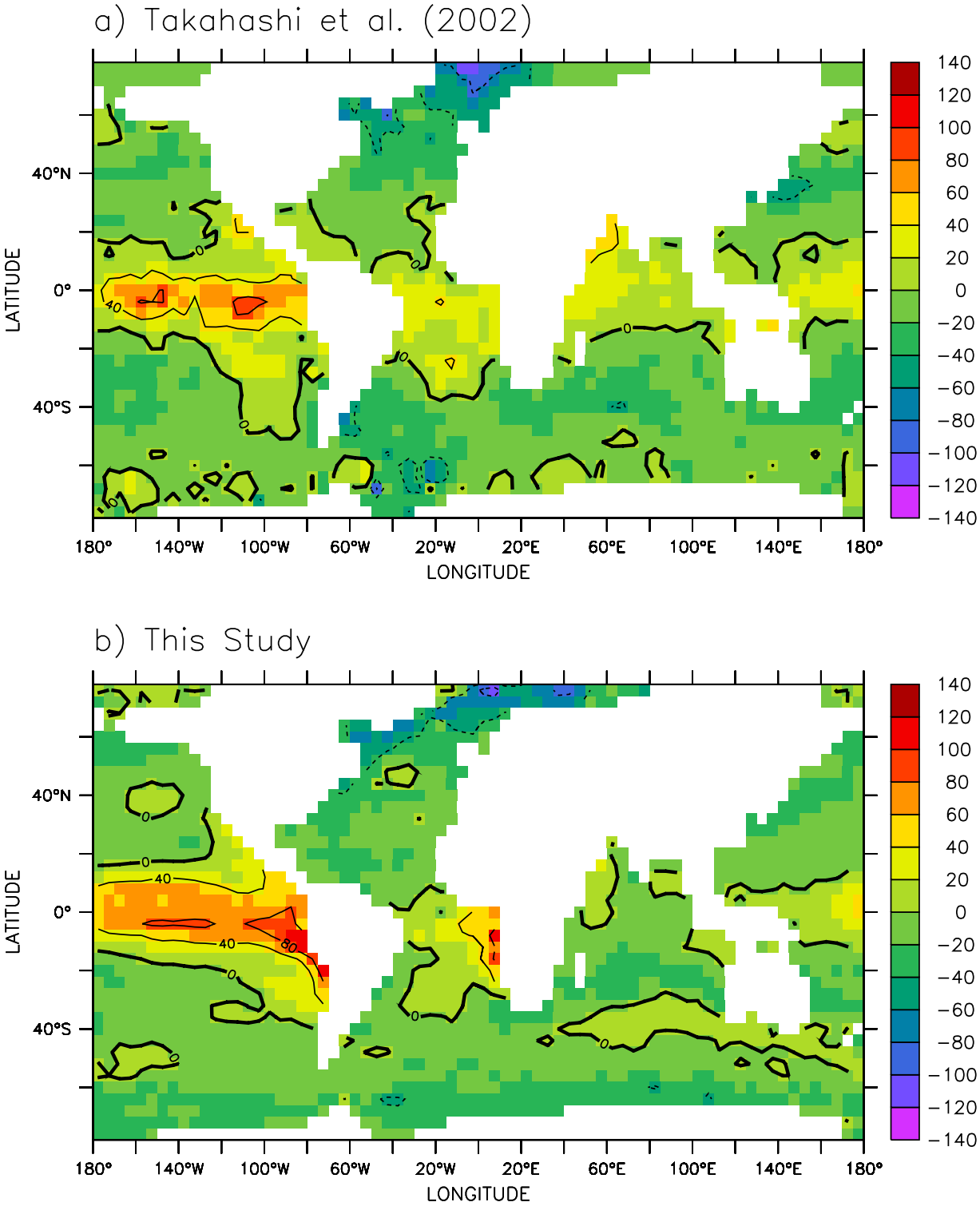

Figure 3. (a) Mean ΔpCO_2 values from *Takahashi et al.* [2002], computed for the reference year 1995 in ppm. (b) Mean ΔpCO_2 of the year 1995 of the anthropogenic run in ppm; interpolated to the 4° × 5° grid of *Takahashi et al.* [2002].

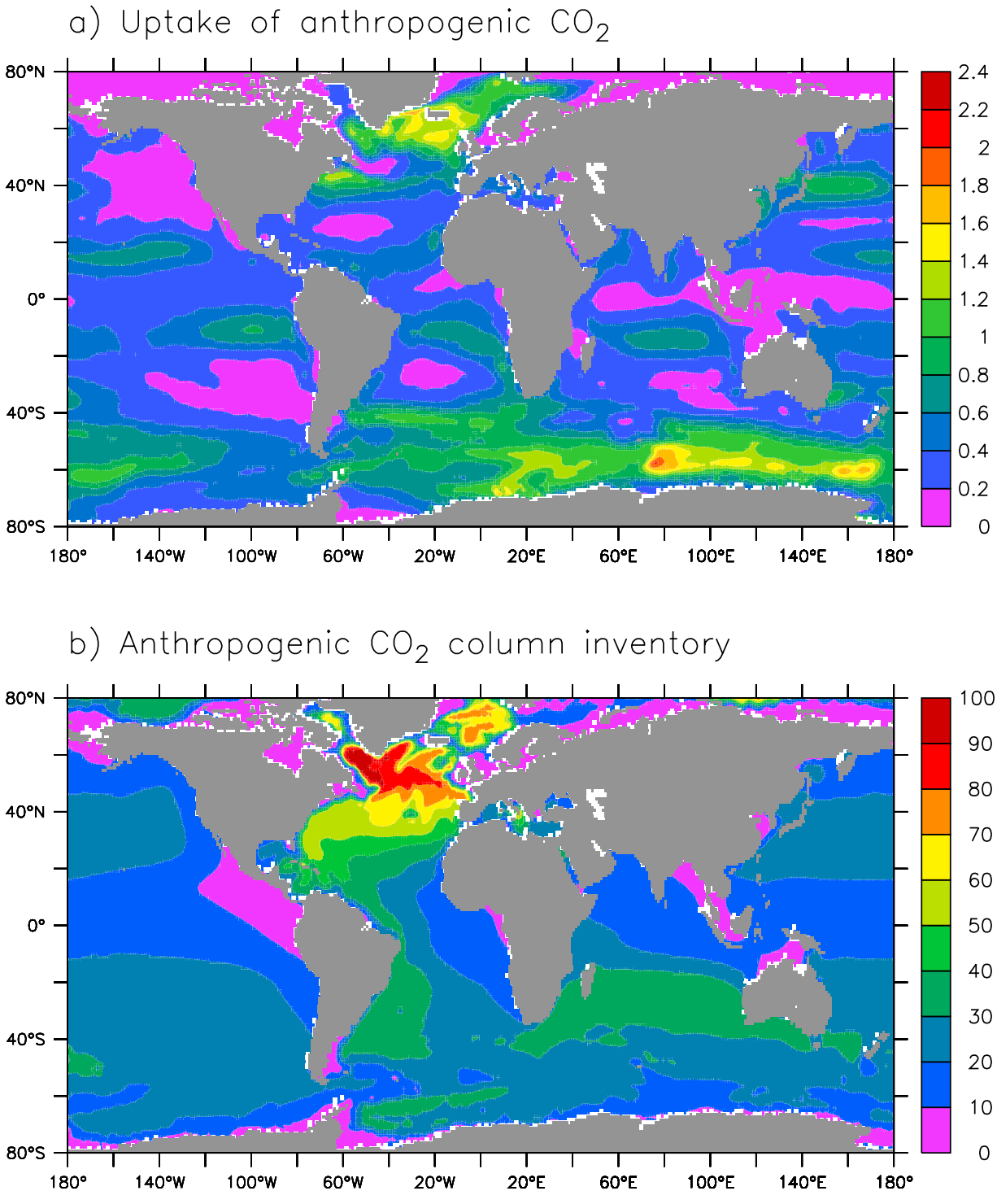

Figure 5. (a) Mean anthropogenic CO_2 uptake for 1990–1999 in mol C m^{-2} yr^{-1}. (b) Mean column inventory of anthropogenic CO_2 of the year 1995 in mol C m^{-2}.

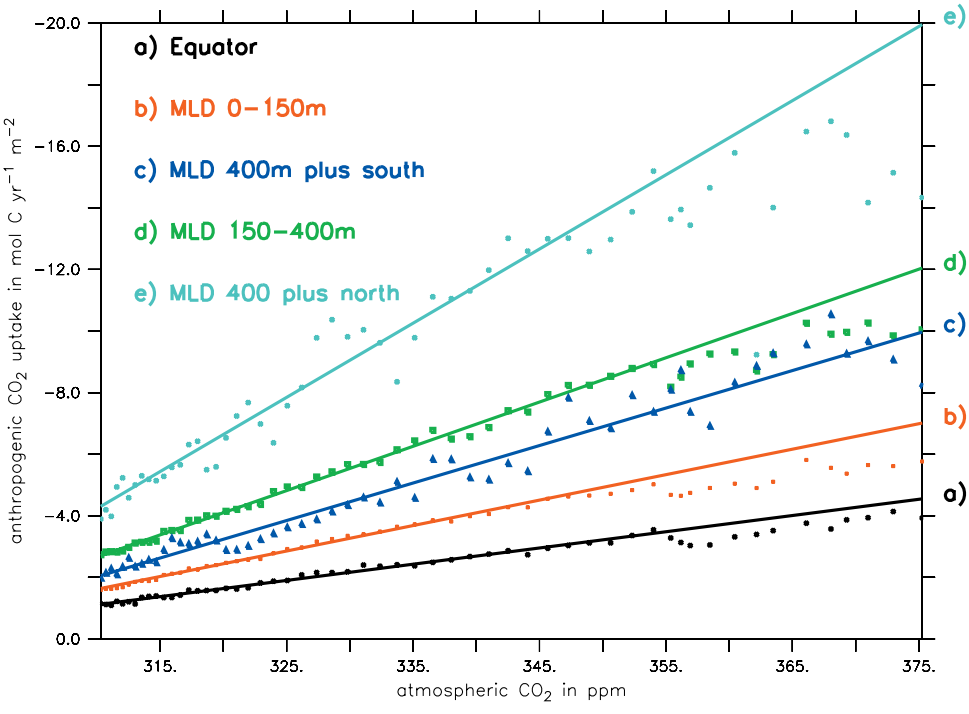

Figure 6. Yearly averages of anthropogenic CO_2 uptake versus atmospheric CO_2 concentrations. The uptake rates are computed for the equatorial regions, regions with an average mixed layer depth of up to 150 m, 150 m to 400 m, and over 400 m in the Northern and Southern Hemisphere. The linear regression lines are computed for 310 ppm to 345 ppm and extended over the full range.

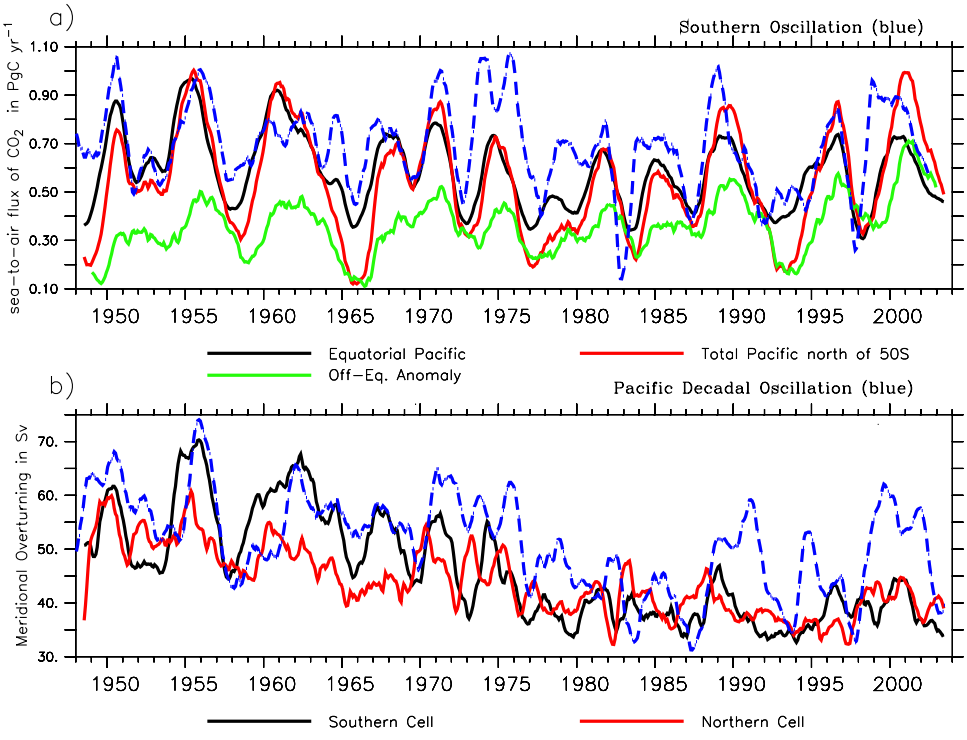

Figure 8. (a) Sea-to-air CO_2 fluxes of the control run (smoothed with a 12-month running mean) of the total Pacific and of equatorial Pacific from 10°N to 10°S and 80°W to 135°E. The Southern Oscillation Index is shown in blue. (b) Overturning of the southern and northern Equatorial Cell in the Pacific. The Pacific Decadal Oscillation Index is shown in blue.

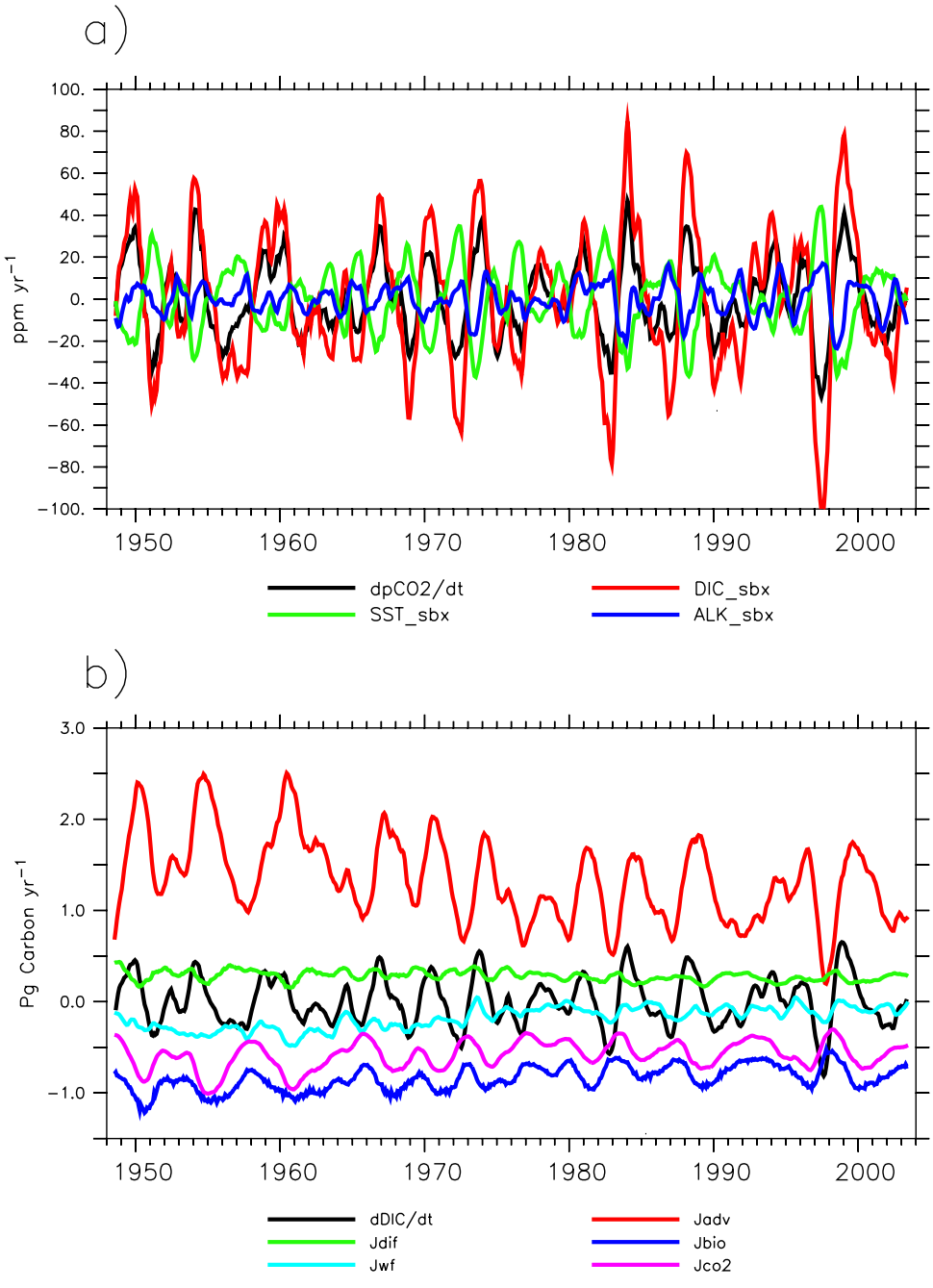

Figure 9. (a) Component analysis for the terms of equation (3) in the surface box of the equatorial Pacific from 10°S to 10°N and 80°W to 135°E. (b) Components of equation (4) for the upper 42 m of the same area. All fluxes are from the control run and smoothed with a 12-month running mean.

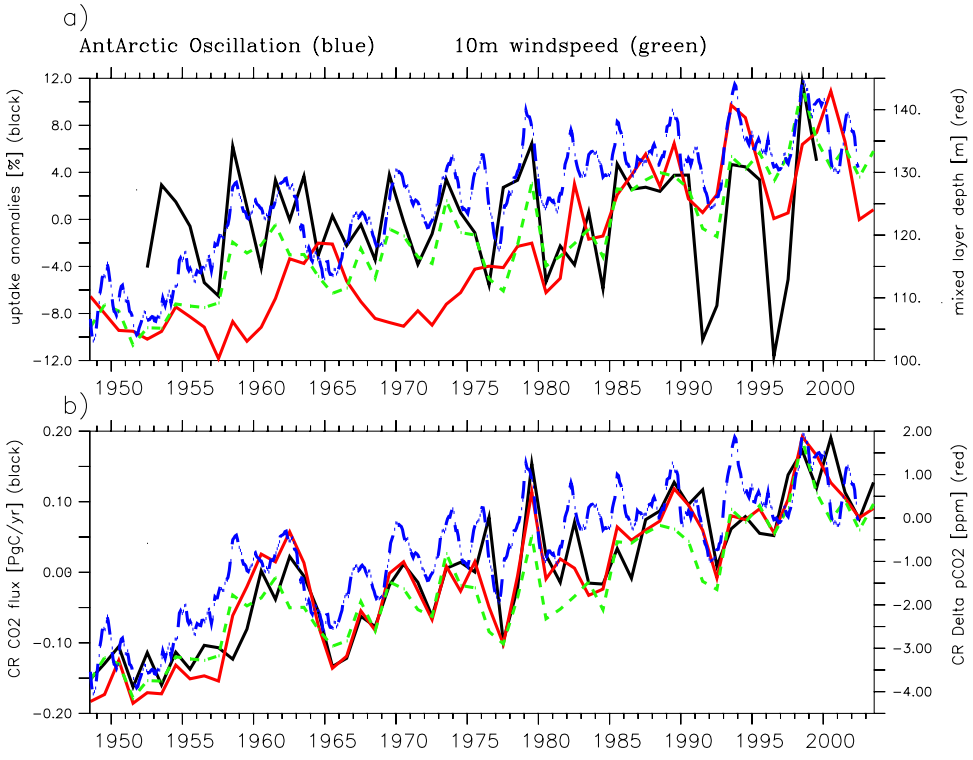

Figure 11. Yearly means for the Southern Ocean from 40°S to 60°S. In blue is the Antarctic Oscillation Index, and in green is the 10-m wind speed from the NCEP reanalysis. (a) Anomaly in the uptake of anthropogenic CO_2 (AR experiment) and carbon transported into the upper 42 m by advection and diffusion (components of equation (4). (b) CO_2 flux and ΔpCO_2 from the control run (CR).

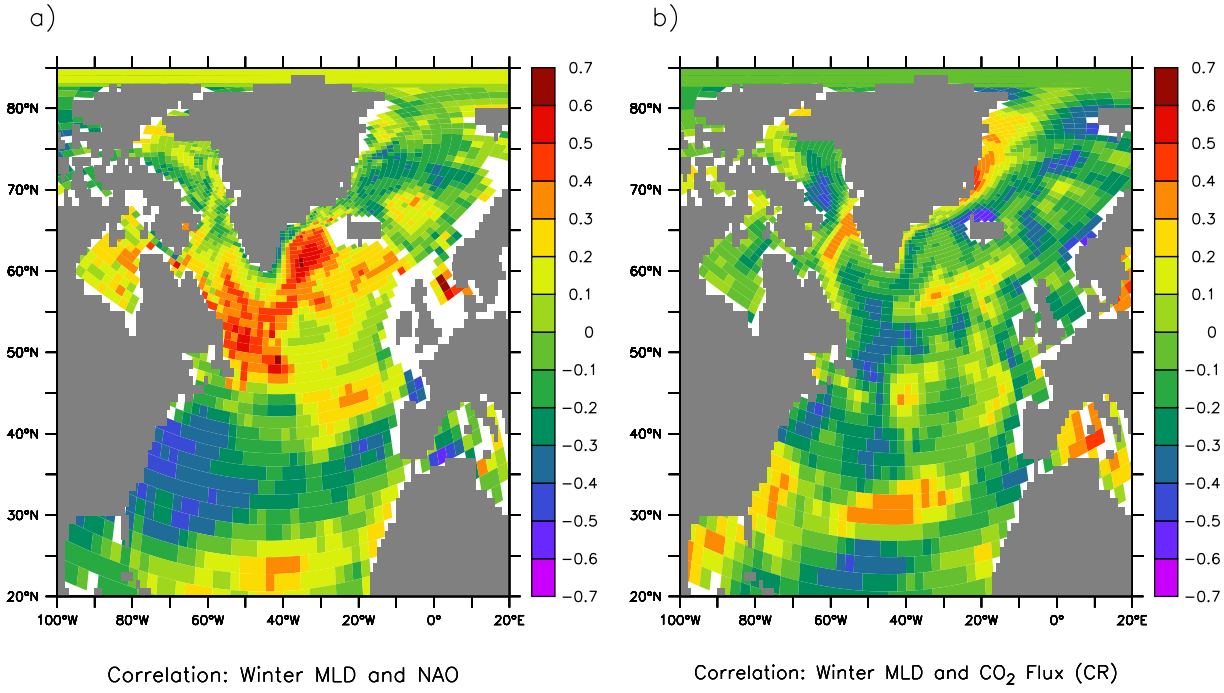

Figure 13. Correlation of the wintertime North Atlantic Oscillation (NAO) with (a) winter mixed layer depth and (b) mean sea-to-air CO_2 flux anomalies from the control run (CR).

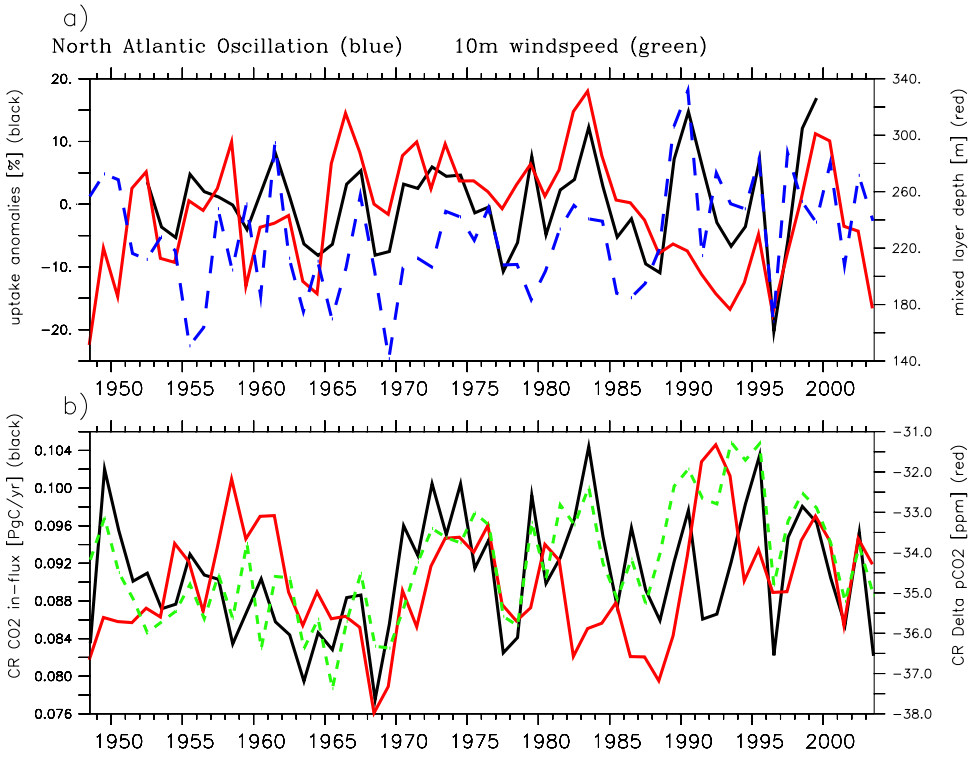

Figure 14. Yearly means for the Greenland, Iceland, and Norwegian seas. In blue is the North Atlantic Oscillation Index, and in green is the 10-m wind speed from the NCEP reanalysis. (a) Anomaly in the uptake of anthropogenic CO_2 (AR experiment) and the average mixed layer depth. (b) CO_2 in-flux and ΔpCO_2 from the control run (CR).

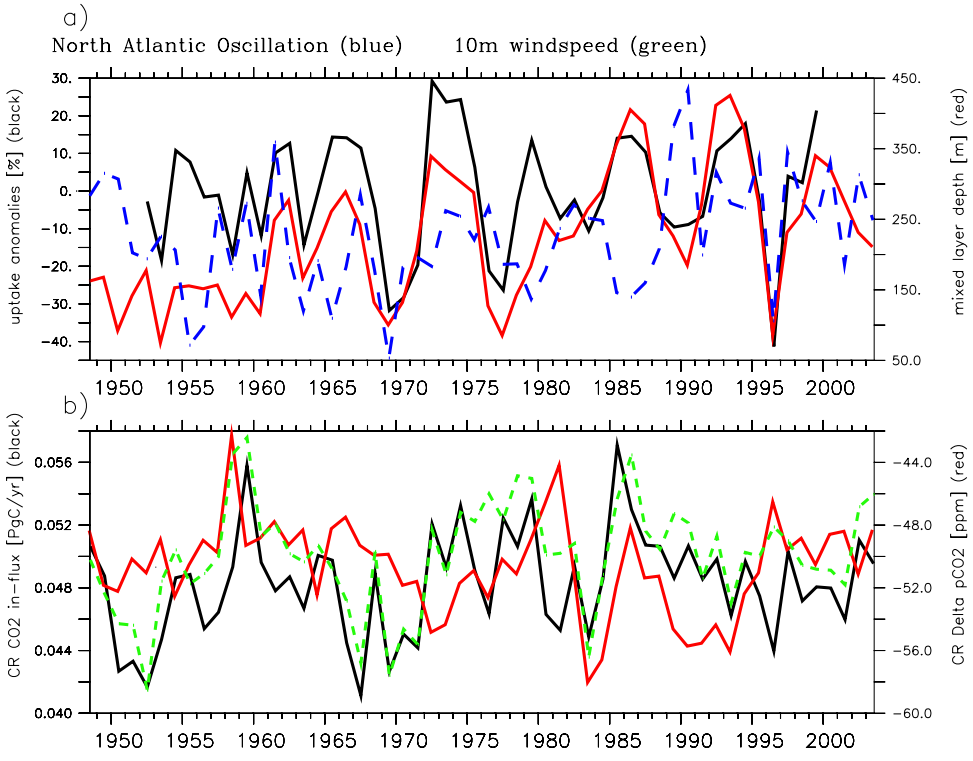

Figure 15. Yearly means for the Labrador Sea. In blue is the North Atlantic Oscillation Index, and in green is the 10-m wind speed from the NCEP reanalysis. (a) Anomaly in the uptake of anthropogenic CO_2 (AR experiment) and the average mixed layer depth. (b) CO_2 in-flux and ΔpCO_2 from the control run (CR).